Short-circuit Contributions from Fully-rated Converter Wind Turbines

Modeling and simulation of steady-state short-circuit contributions from FRC wind turbines in offshore wind power plants

JOAKIM AHNLUND

KTH Electrical Engineering

Degree project in
Electric Power Systems
Second Level,
Stockholm, Sweden 2014

XR-EE-EPS 2014:004

ROYAL INSTITUTE
OF TECHNOLOGY

Short-circuit contributions from fully-rated converter wind turbines

Modeling and simulation of steady-state short-circuit contributions from FRC wind turbines in offshore wind power plants

JOAKIM AHNLUND

Master's Thesis at EES
Supervisor: Amin Nasri
Examiner: Mehrdad Ghandhari

April 2014

Abstract

In recent years there has been an increase in wind power plants installed out at sea. The generated power of wind turbine generators (WTGs) are collected through numerous subsea cables into a single hub, the offshore platform. Subsequently, this platform is interconnected with the onshore main grid through a further stretch of cable. In the event of a fault, a sudden increase in current, so called short-circuit current, will occur somewhere in the system. The short-circuit current will, depending on the duration and location of the fault, potentially harm the power system. In order to accurately determine the dimensions and rating of the equipment installed in the offshore wind power plant (OWPP), the magnitude of this current needs to be studied. Furthermore, depending on the country in which the OWPP is installed, the transmission system operator (TSO) might pose different low-voltage-ride-through (LVRT) requirements on the system. One such requirement is that the installed turbines should provide voltage regulation through injection of reactive current. A type of generator able to achieve this is a so-called fully-rated converter wind turbine generator (FRC WTG). Through a power electronic interface, the reactive and active current components of the generator can be freely controlled. With a high level of reactive current injected during a fault in the OWPP, the short-circuit contribution from these FRC WTGs needs to be evaluated. In this master's thesis, a method has been developed in order to determine the steady-state short-circuit contribution from multiple FRC WTGs. This methodology is based on an iterative algorithm, and has been implemented in the simulation tool PowerFactory. To evaluate the performance of the method, two case studies were performed. In order to improve simulation times, an already existing WTG aggregation model has been implemented to reduce the number of turbines in the test system. From the results, it is concluded that the method obtains the expected FRC WTG short-circuit currents with sufficient accuracy. Furthermore, the deviation from the expected results are evaluated using a numerical tool. This project was initiated and conducted at ABB in Västerås, Sweden.

Sammanfattning

Under de senaste åren har det skett en ökning av vindkraftparker installerade till havs. Den genererade effekten från varje enskild vindturbin samlas upp via havskablar till en platform där den transformeras till en högre spänningsnivå. Från platformen transporteras effekten sedan vidare in mot land genom en längre kabel som ansluts till en landstation. Landstationen i sin tur är ansluten till stamnätet. I händelsen av ett fel någonstans i system kommer höga strömmar att rusa, så kallade kortslutningsströmmar. Beroende på varaktigheten och platsen för felet kan dessa strömmar vara skadliga för systemet. För att på ett noggrannt sätt bestämma dimensioner och märkvärden på den utrustning som ska installeras i systemet måste därför storleken på denna ström studeras. Utöver detta så kan nätoperatören, beroende på vilket land som vindkraftparken är installerad i, ställa olika krav på hur systemet ska hantera spänningsfall i felsituationer. Ett sådant krav är att vindturbinerna i parken måste bistå med spänningsreglering medelst injektion av reaktiv ström. En typ av vindturbin som klarar av att uppfylla dessa krav är så kallade helomriktade vindturbiner. Via en effektelektronisk frikoppling kan generatorns aktiva samt reaktiva strömbidrag kontrolleras fritt. Då en stor mängd reaktiv ström eventuellt kan injiceras på grund utav en kortslutning i parken måste bidraget från dessa turbiner utvärderas. Under detta examensarbete har en metod för att bestämma det stationära kortslutningsbidraget från ett flertal helomriktade turbiner utvecklats. Metoden är baserad på en iterativ algoritm och har implementerats i simuleringsverktyget PowerFactory. För att utvärdera metodens prestanda har två fallstudier utförts. I avsikt att förbättra simuleringstiden har en redan befintlig metod för aggregering använts för att minska antalet turbiner i testkretsen. Sammanfattningsvis uppnår metoden erforderliga resultat, baserat på de förväntade kortslutningsbidragen från vindturbinerna. De avvikelser som uppträder utvärderas med hjälp av ett numeriskt verktyg avsett för den föreliggande studien. Det här projektet initierades och utfördes på ABB i Västerås.

Acknowledgements

First of all, I would like to thank Ann Palesjö and Magnus Tarle, my supervisors at ABB, for their support and guidance during my thesis project. Especially, I would like to thank Magnus for always taking his time when answering my questions. Besides my supervisors at ABB, I would also like to thank Lars Lindquist, for his insightful feedback during my weekly meetings, Amin, for the final review of my report, as well as my mother, whom have provided me with roof over my head in Västerås.

Joakim Ahnlund
Ludvika, April 2014

Erkännanden

Först och främst skulle jag vilja rikta ett stort tack till mina handledare på ABB, Ann Palesjö och Magnus Tarle, för deras stöd och handledning under mitt examensarbete. Jag skulle även vilja rikta ett extra tack till Magnus som alltid har tagit sig tiden att sätta sig ned och besvara de frågor som jag haft. Utöver mina handledare på ABB skulle jag också vilja tacka Lars Lindquist, som bidragit med sin kunskap under mina veckomöten, Amin, för den slutgiltiga granskningen av min rapport, samt min mor, som bistått med tak över huvudet i Västerås.

Joakim Ahnlund
Ludvika, April 2014

Contents

Chapter 1

Introduction

1.1 Background

In order to reduce green house gas emissions, the European Union has initiated the climate targets known as *20-20-20*, as a part of the Europe 2020 strategy [1]. These targets state, that by the year 2020 the following goals should have been achieved by the union in whole; a 20 % reduction in greenhouse gas emissions from 1990 levels, an increase in the amount of energy consumed from renewable energy sources by 20 % and a 20 % improvement in overall energy efficiency [2]. The demand for renewable energy is not only dictated by goals such as these, but also out of a safety perspective. As a reaction to the Fukushima incident in 2011, Germany decided that all nuclear power within the country should be phased-out by 2022. Furthermore, the energy produced by renewables should amount to 35 % by 2020 and 80 % in 2050, according to the country's climate goals [3]. In order to meet this growing demand for renewable energy, the penetration of unconventional technologies such as solar and wind power is expected to further increase [4].

To utilize the energy in the wind more efficiently, Offshore Wind Power Plants (OWPPs) are installed at sea where wind velocities are higher, there are less issues with land use and towers heights can be lower [5]. These plants are connected to the onshore main power grid through undersea cables, which enables the remotely generated electricity to be transmitted to the location where it is to be consumed. When designing such a plant, there are multiple aspects that need to be taken into consideration. System components need to fulfill requirements, while the plant itself needs to interact with the onshore power grid in a non-detrimental way. Examples of design studies that help to define these requirements are:

- Load-flow studies: Equipment ratings need to be according to the planned output power of the OWPP. Cables and substation components should be dimensioned accordingly to avoid over-heating and electrical breakdowns caused by high currents and voltages, which could permanently damage the equipment.

- Harmonic studies: Based on requirements of the Transmission System Operator (TSO), harmonics injected into the main grid need to be kept below specified values. The components installed in the OWPP should also be able to handle the harmonics absorbed from the main grid, or the existing background harmonics amplified by the export cable. Theses studies also deal with the requirements set for the amplification of background harmonics. Harmonics can be mitigated using filters.

- Temporary overvoltage studies: The High Voltage Alternating Current (HVAC) export cables installed between the offshore platform and the main land will amplify voltage distortions in the main grid, causing overvoltages in the OWPP [6].

- Short-circuit and fault studies: In the event of a fault in the main grid, or in the OWPP, system components need to be able to withstand high currents and over-voltages caused by the short-circuit.

In any type of system design, it is important that the type of requirements mentioned above are fulfilled, out of both a safety and operational perspective. The system design engineer could therefore always pick components that have higher ratings than what is observed in the studies, to be on the safe side. In order to minimize costs, however, it is important that components are selected in such a way that system requirements are fulfilled, while avoiding over-dimensioning of the system. The design engineer therefore needs to decide on a trade-off between these two aspects, to be able to perform reliable system studies.

One of the key components in an OWPP is the Wind Turbine Generator (WTG). One type of WTGs utilized in modern OWPPs, are so called Fully-Rated Converter Wind Turbine Generators (FRC WTGs), which are interconnected to the system by power electronic converters [7]. These converters are able to control the power angle of the generator, i.e. the amount of active and reactive current provided by each generator. In the event of a short-circuit, the converter can provide voltage support to the grid by injecting reactive current, and thus, resulting in a controlled short-circuit current. The behavior of FRC WTGs during a fault will therefore be quite different, as compared to conventional turbines based on asynchronous and synchronous generators without power electronic converters. It is safe to assume that there will be an increased share of FRC WTGs in the future which makes current industry standards used for short-circuit calculations obsolete. It is also plausible that a portion of new generation large-scale OWPPs will consist entirely of FRC WTGs, as these comply with national grid codes defined by the TSO. These grid codes contain requirements on the Low-Voltage-Ride-Through (LVRT) capability of a WTG, i.e. the generators' ability to remain connected during a low voltage dip and provide support to the grid through reactive current injection. When performing short-circuit studies of any such system mentioned above, the short-circuit

contributions from FRC WTGs need to be taken into consideration, as the accumulated reactive current injected by the turbines during the fault is non-negligible.

This thesis project was initiated by the system design group at Offshore Wind Connections, part of the Power System Division at ABB (OWC), ABB, Västerås. Prior to the project a pre-study was performed within the company by ABB employee Johan Carlsson.

1.2 Purpose

A complete OWPP system design performed by ABB includes all components from the Point of Common Connection (PCC), to the high voltage terminal of the WTG transformer. The choice of WTG type and manufacturer is not included in this design, and thus, handled separately by the customer. For system designs including FRC WTGs, the short-circuit behavior of the turbine generator therefore has to be assumed to comply with grid code regulations, and based on provided WTG manufacturing data. There are numerous dynamic models showcasing this behavior, e.g. [8, 9], and similar studies could be performed if a similar dynamic model was provided by the WTG manufacturer. In the process of designing an overall system, however, it is unpractical to perform such studies. In order to cover all relevant short-circuit cases, a great number of different configurations and fault locations need to be investigated, including normal operation setup and contingencies. The process of setting up, running and evaluating dynamic simulations for a great number of WTG models, given these circumstances, should therefore be avoided.

When performing short-circuit studies for systems including conventional turbine types, the industry standard IEC 60909 [10] is widely accepted. The IEC 60909 standard is a conservative method and is primarily used to determine the *steady-state* short-circuit current. From the results other relevant quantities, such as the transient peak current, are derived. This standard is, along with many other, implemented in the power system tool *PowerFactory*. The software is developed by German DIgSILENT (Digital SimuLator for Electrical NeTwork), and is the tool used by the system design group at OWC for short-circuit calculations. In addition to conventional standards, DIgSILENT has developed a complete short-circuit calculation method based on the IEC 60909 standard [11]. By using a static calculation method, the dynamic short-circuit behavior of FRC WTGs could be approximated in a similar fashion.

The purpose of this thesis project is to develop and implement a steady-state short-circuit calculation method in PowerFactory. The method should be aimed towards Offshore Wind Power Plants utilizing Fully-Rated Converter Wind Turbine Generators.

1.3 Previous Work

There are numerous sources found in the literature dealing with the intricate details of reactive power requirements of OWPPs and grid code compliance [12–16]. The Dynamic Voltage Support (DVS) required during LVRT dictated by national grid codes in different countries, are summarized in [17]. The time-depending LVRT stipulated by a national grid code provides a required voltage profile, which must be sustained during the fault period. At a specific level of the recovery voltage, however, the FRC WTG need to inject reactive current. For a given voltage drop at the terminal, a specific Root Mean Square (RMS) reactive current value in p.u. is defined by the grid code. In [17] the reactive current injection curves used by Spain, Germany and Denmark for DVS are compared. Both the German and Danish grid codes are based on a linear curve within a set voltage range, while the Spanish curve is piece-wise linear. The German and Spanish grid codes also define the reactive power absorption during high voltages. When designing an OWPP, the short-circuit behavior of the FRC WTGs must comply with the above grid code requirements. The short-circuit models used for the generators must therefore reflect the physical behavior of the converters, as these control the active and reactive current injection during a fault.

The dynamic short-circuit behavior of conventional WTGs can be found in [18]. In the article, generic generator models of type 1, 2, 3 and 4 are developed and used in dynamic short-circuit simulations for faults at the WTG terminal. Here, generators of type 1 - 3 can be considered as conventional topologies while type 4 refers to FRC WTG. The resulting behavior of each generator type is compared with an emphasis on type 1 - 3 generators. The authors conclude that the highest short-circuit currents occur for three-phase-to-ground faults, but also that this type of fault is rare compared to single-line-to-ground faults in an OWPP. The DVS of the type 4 generator during low terminal voltages is not explored. The dynamic short-circuit behavior of the FRC WTG is concluded to act as a symmetrical current, limited to 1.1 times the rated converter current, for all types of faults used in the study. This is due to the power converter's ability to control all three phase currents independently.

Studies have been performed where the dynamic behavior of converter controlled WTGs have been modeled and simulated. In [8] different control strategies used by FRC WTG during LVRT for both HVAC and High Voltage Direct Current (HVDC) systems are developed and compared. The voltage recovery of the HVAC system is showed to be improved by the reactive current injection provided by the WTG converter. Yet another control strategy used for FRC WTGs is developed and simulated in [9]. This study is a further example of the utility of FRC WTG. Attempts at providing DVS during LVRT by the implementation of a crowbar circuit in a Doubly-fed Induction Generator (DFIG) is illustrated in [19]. In [20] the conventional delimitation between subtransient, transient and steady-state short-circuit currents are discussed in relation the controlled behavior of the short-circuit cur-

rent of a FRC WTG. The author argues that these time lineations do not exist for the FRC WTG and that "*...there is no need to distinguish between a "subtransient" response and transient response*"[20].

The above references only serve as a background to the project, and has little to do with the task of performing steady-state short-circuit calculations. Previous work performed within this specific field has proven to be scarce. The only relevant work found during the literature review is summarized below.

Prior to this project, the thesis *Fault Current Contribution from VSC-based Wind Turbines to the Grid* was presented in 2008 by Valentini Massimo [21]. The steady-state short-circuit contribution from a FRC WTG was modeled and implemented in PowerFactory, using an iterative algorithm. The WTG was modeled using a Thévenin equivalent, i.e. a voltage source in series with an impedance, and was implemented in accordance with minimum requirements of the German grid code. To verify the model it was tested in a Single-Machine Infinite Bus (SMIB) system, and compared with simulation results from a Siemens WTG. A case study was performed, where the method was implemented and used in a system model of the Nysted/Rødsand OWPP. The method developed within the project was never used for a OWPP utilizing solely FRC WTGs, or an array of non-aggregated WTGs. In addition to the novel work presented in the report, an extensive analysis of the requirements of LVRT, and DVS capabilities according to a number of national grid codes, was performed, as well as a review of the short-circuit calculation methods available in PowerFactory.

In 2012 an iterative method similar to the one described by Valentini Massimo was proposed by Si Chen et al. [22]. The model was based on the static generator model implemented in PowerFactory, and was used to illustrate the effects of DVS. The static generator model is intended to be used both for load flow and dynamic simulations of a FRC WTG. The short-circuit behavior is modeled by a short-circuit power and impedance ratio X''/R. In [22] these two parameters are changed iteratively until the method converges, or the short-circuit power exceeds six times the rated power of the generator. The method was developed for the Danish TSO *Energinet.dk*, and served to comply with the reactive current requirements according to grid code requirements in Denmark [23]. The iterative method was compared to results obtained using the complete method and IEC 60909 in PowerFactory, for a study case of the DK1 system in Denmark. Results showed how the total short-circuit power obtained by the iterative method, at the 400 kV substation, was considerably higher as compared to results obtained using the IEC 60909 standard, and marginally higher than results obtained using the complete method. Furthermore, the resulting internal impedance of different wind power plants during the short-circuit was lower when using the iterative method, as compared to the complete method.

In August 2011, version 14.1 of PowerFactory was released. The new version included a current iteration functionality incorporated in the complete method [24]. According to DIgSILENT, this method uses an iterative algorithm to determine the steady-state short-circuit current of the static generator model included in the software. The documentation for this new functionality leaves much to be desired and Digital SimuLator for Electrical NeTwork (DIgSILENT) are yet to release benchmark tests. A brief introduction to the implemented method can be found in [25]. Through a current iteration loop, the resulting transient current contribution I'_k of the FRC WTG is obtained based on the slope K of the grid code voltage control curve, and a maximum allowed WTG short-circuit current. Furthermore, the method is reported by DIgSILENT to normally converge within 5-10 iterations.

1.4 Problem Definition

When performing simulations using the current iteration method implemented by PowerFactory, it has been noted that only the resulting transient short-circuit current $\boldsymbol{I'_k}$ is reported. The flow of reactive and active power, bus voltages and the corresponding phasor angles during the short-circuit are based on the subtransient short-circuit model used by the complete method. Consider the example found in figure 1.1. All simulation results except the transient short-circuit current *Iks*, and the corresponding current angle *phiiks*, are related to the subtransient short-circuit current. The power angle *phiui* is the residual angle of *phiu* and *phii*

$$phiui = phiu - phii = -5.065^\circ - (-42.588^\circ) = 37.523^\circ$$

With a bus voltage of 690 V, the resulting short-circuit power is

$$\begin{aligned} \boldsymbol{S} &= u \cdot 690 \text{ V} \cdot \sqrt{3} \cdot Ikss \cdot (\cos(phiui) + j \sin(phiui)) = \\ &= 0.4924 \cdot 690 \text{ V} \cdot \sqrt{3} \cdot 67.446 \text{ kA} \cdot (\cos(37.523^\circ) + j \sin(37.523^\circ)) = \\ &= 31.479 + j24.175 \text{ MVA} \end{aligned}$$

The lack of simulation results leaves the user with no way of verifying the obtained transient short-circuit current, which of course is an important matter when utilizing newly implemented software functionality. Furthermore, the implementation is based on a specific grid code, with only two available input parameters. Consider a TSO utilizing a different type voltage control curve, or using FRC WTGs with a regulation curve providing more reactive current than what is stated by the minimum requirements. If system studies are to be performed for such cases, additional input parameters need to be considered.

In order to correctly simulate the expected short-circuit contributions from FRC WTGs and/or validate the method developed by DIgSILENT, a separate method needs to be used. Such methods are proposed in [21] and [22], i.e. the previous projects discussed in Section 1.4. These methods are however not suitable for the

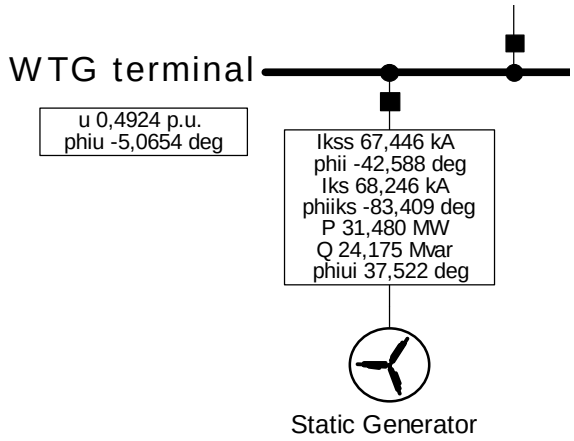

Figure 1.1. *Example of short-circuit simulation results obtained using the static generator model in PowerFactory with current iteration.*

purpose of this project. First of all, neither of them are implemented for multiple WTGs which is required for a full short-circuit study of a large-scale OWPP. Secondly, the method proposed by Chen, S. et al. is ruled out because of the restrictions in using an iterative method based on the static generator model, in combination with the complete method in PowerFactory. In the algorithm, the short-circuit power of the static generator is assumed to be six times the rated power of the generator. When designing different systems utilizing varying types of FRC WTG, this limitation will depend on the manufacturing data of the turbine.

At this point it is tempting to expand the method proposed by Valentini, M. to incorporate multiple WTG models. The method is, however, considered inappropriate for the purpose of this project, based on the following

1. The method has convergence issues or is unable to converge for terminal voltages above 0.8 p.u. and below 0.1 p.u.

2. The method has only been implemented and tested for the minimum requirements of a specific grid code voltage control curve.

3. The convergence time of the method when applied to a SMIB sometimes approaches 10 seconds.

There are two major issues related to the first of the above points. It is not always safe to assume the fault impedance to be such that the remaining voltage at the WTG terminal is 0.1 p.u. or above. Assume that a bolted or low-impedance fault occurs at the low voltage side of the WTG transformer, i.e. directly at the generator terminal. The voltage during such a fault is likely to drop below 0.1 p.u.. For a full short-circuit study, such faults need to be considered. Also consider an OWPP

where two or more arrays of FRC WTGs are separated by cable and transformer impedances. In figure 1.2 a simplified example is provided. Two WTGs are connected by large impedances to a common bus, which subsequently is connected to a strong grid through yet another impedance. A bolted or low-impedance fault occurs at the left WTG terminal, which results in a voltage drop below 0.1 p.u.. The resulting short-circuit current from the grid connection is so high that the retain voltage at the right WTG terminal stays above 0.9 p.u.. Even if the high terminal voltage case is of little interest when dealing with an isolated generator, it needs to be modeled correctly for a large system, since these currents will interact with the resulting short-circuit. It is therefore important to successfully include the behavior of the FRC WTGs for high terminal voltages in the model as well. In other words, the model needs to be able to handle terminal voltages above 0.8 p.u. and below 0.1 p.u..

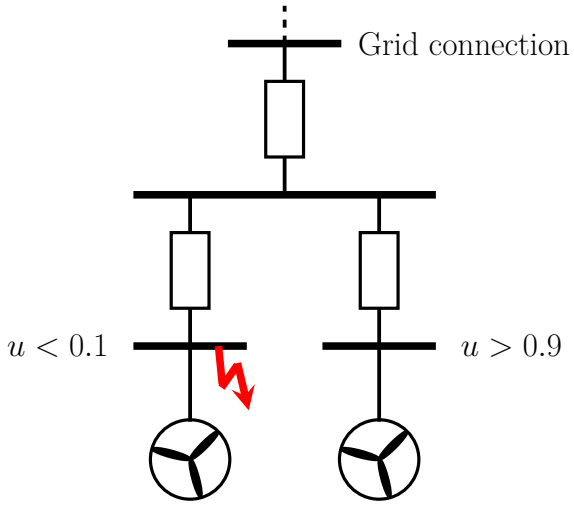

Figure 1.2. *Example of two WTGs separated by considerable impedances.*

The control algorithm used for DVS will depend on the WTG manufacturer, choice of algorithm, type et cetera. This is not the case according to the second point in the previously mentioned list. For instance, if the control algorithm of the FRC WTG provides more reactive current than what is specified by the minimum grid code requirements, this needs to be accounted for in the model.

When performing short-circuit simulations for multiple FRC WTGs, which cannot be aggregated, the convergence time of each separate model will start to affect the choice of method. This is the case mentioned in the third point above. This issue should, however, be considered minor compared to the aforementioned.

In order to accurately model the short-circuit behavior of multiple FRC WTGs

interconnected in a large OWPP, a consistent method needs to be developed. One partial goal of this thesis is therefore to cover the short-comings mentioned above.

1.5 Objectives

The method developed for this project should determine the steady-state short-circuit contribution from each FRC WTG in an OWPP, based on the reactive current injection dictated by grid code regulations. This will be achieved through the implementation of an outer loop, dealing with the individual current contribution from each turbine, and an inner loop which iterates through all available turbines assuring an overall accurate system solution. The method implementation in PowerFactory should allow the user to adjust the grid code reference curve through different input parameters, and should be adjustable to different WTG manufacturer specifications. For instance, if the turbine provides more reactive power than what is required by minimum grid code requirements, this should be obtainable by the use of such an input parameter.

The method will be used for worst-case scenarios, i.e. system configurations that will result in the highest short-circuit current for a specific component. The method is only to be used for Alternating Current (AC) based OWPPs. Beside the steady-state short-circuit current, the following contribution from each turbine should also be determined

- Decaying DC component, $i_{d.c.}$
- Symmetrical short-circuit current, I_b
- Thermal equivalent current, I_{th}

The calculation of the transient peak current i_p is left for future studies.

The study is carried out based on the following restrictions:

- The OWPP is connected to a strong or stiff grid. The most important implication of this is that the short-circuit current from the grid will constitute a considerable portion of the total short-circuit current in the OWPP.
- The OWPP only consists of FRC WTGs of the same rating and manufacturer.
- Each WTG is operated at its rated output power during steady-state operations.
- Only three-phase line-to-ground faults are considered.
- The grid is assumed to be mainly inductive, resulting in a mostly inductive short-circuit current.

Since this method is to be used for steady-state short-circuit calculations, the results will be of an approximate nature, and measures should be taken to assure that the obtained results remain conservative within reasonable bounds. Furthermore, the modeled behavior of the FRC WTG is assumed to be ideal. Meaning that the physical WTG used in the design, will comply with the grid code voltage control curve.

1.6 Contributions

In Section 3.3 a new iterative method used for the calculation of the steady-state short-circuit current I_k is presented. The method is implemented using the AC current source in PowerFactory, and can be used for any system model including multiple FRC WTGs. From simulations the transient short-circuit current I'_k is obtained, which for this study will be equal to the steady-state current I_k. Current contributions based on I'_k of each turbine are also included in the model, i.e. i_{DC}, I_b and I_{th}. In order to handle a large number of WTGs within the system, an aggregated model has been utilized, where the impedance aggregation has been implemented based on [26]. The reference grid code requirements are based on a linear slope which saturates for the maximum value of the reactive current. Beside setting these values freely, the user can set the dead band voltage, as well and a minimum reactive current, greater than that of the requirements of the linear slope. In order for the iterative method to converge for the discontinuity caused at the dead band, a polynomial smoothing function has been introduced. The user has the option to alter the smoothness of the function through a free selection of the polynomial factor n. Also included in the method is the post-calculated deviation factor δ. This is a measurement of the deviation from the unknown, "true", value which is expected from a real-life system, and serves to account for short-comings of the developed method. Furthermore, δ is used as part of a compensation factor which will provide a conservative estimate of the actual short-circuit current obtained.

In order to verify the method and provide an example of its use, two case studies were performed. The first one is found in Section 4.1 and is based on a SMIB test system, i.e. a single generator connected to a slack bus. The system is subject to faults at both the generator and slack bus terminal for a range of fault impedances, such that generator terminal voltages from 0 - 1 p.u. are obtained. The same tests are performed for the static generator model, where current iteration has been used in order to evaluate the difference in results in relation the developed current source method.

The second case study can be found in Section 4.2. A larger test system illustrating a fictional OWPP is introduced and subjected to bolted faults at different locations. The purpose of this study is to illustrate how the newly adopted current source

method is to be used for worst-case short-circuit scenarios, and how the deviation factor δ will depend on different factors.

1.7 Outline

In Section 2, an overview of OWPPs is provided and the concept of short-circuits in OWPPs is further introduced. In Section 3, the IEC 60909 standard, and the short-circuit calculation methods in PowerFactory, are described. This is followed by an in-depth description of the current source method developed for this thesis. In Section 4, two case studies are carried out to evaluate, and illustrate the performance, of the newly presented method. In Section 5, a summary of the thesis is provided along with some general conclusions and recommendations. This is followed by a discussion on the future studies.

Chapter 2

Offshore Wind Power Plants

In this chapter, a brief topological overview of an OWPP is provided. Different turbine technologies are presented alongside an introduction to fault requirements for offshore WTGs.

2.1 Overview

The purpose of a large-scale OWPP, is to transport the electricity generated by the wind turbines out at sea, to the main grid. The benefits of OWPPs, as compared with the onshore counterpart, are summarized in [5]:

- Mean wind speed is approximately 25 % higher.
- Wind shear is lower.
- Higher wind speeds are obtained at lower altitudes, which allows for lowering of the tower height.
- Low turbulence intensity in the dominant wind direction.
- Less restrictions caused by noise, landscape, birds and electromagnetic interference.
- Less issues with land acquisition.

The disadvantages, on the other hand, are higher installation and maintenance costs.

In figure 2.1, the conceptual layout of an OWPP, and its main land connection are illustrated. Numerous WTGs are connected in series to an array cable, which serves to transport the energy from the WTG array to the offshore platform. Each turbine is normally operated in the voltage range 0.4 - 0.9 kV, and is connected to the series array cable through a transformer. The series array cable interconnecting the WTGs must be able to withstand the sum of all operating currents provided by each

turbine, since these are adding up along the length of the cable. Each array cable is connected to an offshore substation at the offshore platform. These substations consists of conventional equipment such as transformers, breakers and shunt capacitances. The offshore transformer installed in this substation is further increasing the voltage level of the transmitted power, in order to reduce power losses dissipated in the subsea export cable connected to the mainland. Usually each transformer is connected to multiple WTG arrays, forming a so called collection grid. As an example, the collection grid in figure 2.1 is made out of four separate WTG arrays.

Depending on how the OWPP is planned and designed, there may be multiple offshore platforms and subsea export cables in the system. These may be interconnected such that the power can be transmitted through one single substation and cable during maintenance or contingencies. On land, the export cable is connected to a larger substation interconnecting the offshore system to the main grid. The point at which the system is connected to the main grid is usually referred to as the PCC. The onshore substation usually consists of a range of standard equipment, such as protection devices, reactive power compensation, filters etc. as well as an onshore transformer. The onshore transformer further increases the voltage to the nominal voltage of the PCC. The transformers used within the system can be of either 2- or 3-winding type, with or without On-Load Tap Changers (OLTCs). The OLTCs are used to adjust the turns ratio at either the low or high voltage side of the transformer, in order to account for operational deviations in the system.

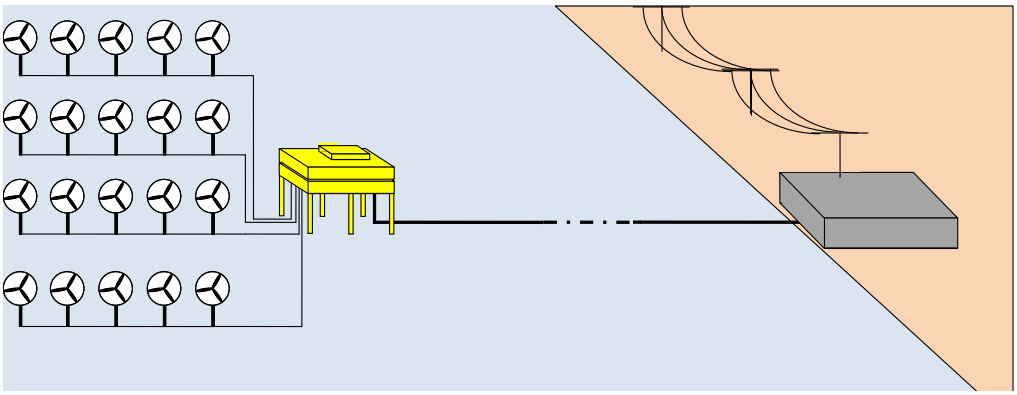

Figure 2.1. *Conceptual illustration of an OWPP.*

2.2 Fully Rated Converter Wind Turbine Generators

In order to convert the kinetic energy in the wind, WTGs are used. These generators are propelled by the motion of the rotor blades attached to the turbine. There are numerous conventional types of generator technologies used in OWPPs, such as DFIG or Doubly-fed Asynchronous Generator (DFAG), Wound-rotor Induction

Generator (WRIG) and Squirrel Cage Induction Generator (SCIG). These are also referred to as generators of type 1 - 3 respectively. For more in depth descriptions of these generators, the reader is referred to external sources such as [18]. For the purpose of this project, the FRC WTG also known as a type 4 WTG, has been studied. Modern FRC WTG technology is either based on a direct-drive or geared turbine generators [27, 28]. The topological overview of these generators can be found in figure 2.2. The direct-drive turbine type utilizes either an electrically excited ,or Permanent Magnet Synchronous Generator (PMSG), and is characterized by a low rotational speed. In order to produce a high power, the generator therefore needs to generate a high torque. To obtain this, the generator requires a high number of poles, which results in a large turbine size. The rotational speed of the rotor is controlled by the pitch of the rotor blades. The trade-off, as compared with geared generators, is that it requires less maintenance. According to [27], the advantage of using a PMSG based FRC WTG, as compared to a conventional DFIG turbine, is that the efficiency is higher, there is no need for brushes and fault-ride-through capability is less complex.

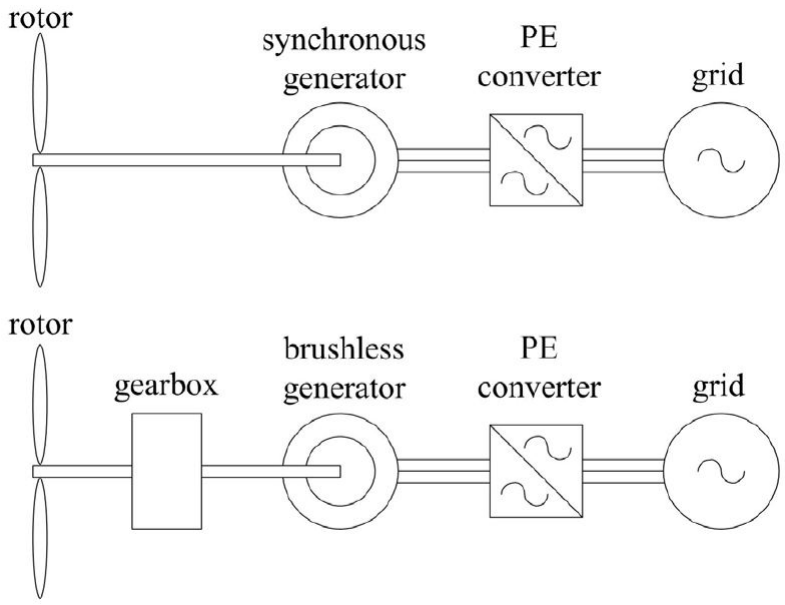

Figure 2.2. *Topological overview of two FRC WTG designs. Source: [28].*

By the inclusion of either a single- or multi-stage gearbox, the rotational speed of the rotor is allowed to exceed that of the direct-drive turbine, while maintaining sufficient torque. To reduce maintenance, the generator technology is commonly based either on a permanent magnet synchronous generator or SCIG, which are both brushless.

In both the case of a direct-drive and geared turbine, the generator stator windings are electrically connected to the grid through a Power Electronic (PE) converter [29]. This allows all of the generated power of the turbine to be controlled and converted by the converter, hence Fully-Rated Converter. Consider the topological overview of a typical Fully-Rated Converter (FRC) in figure 2.3.

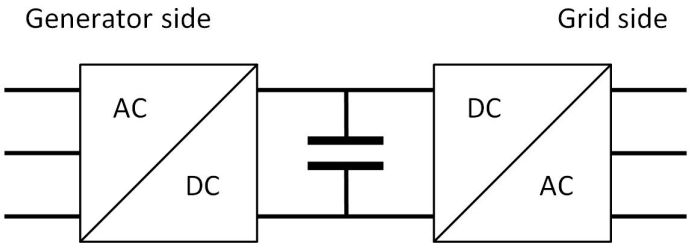

Figure 2.3. *Topological overview of a FRC.*

The FRC generally consists of a generator side rectifier, a DC-link capacitor and a grid side inverter. The DC-link capacitor decouples the generator from the grid, which enables control of the grid side active and reactive power by the inverter [30]. There are numerous PWM-based strategies implemented for the control of the inverter [31, 32]. By enabling almost free control of the grid side current components, the FRC WTG can participate in DVS by injecting reactive current during a fault. The controlled short-circuit current during a fault can therefore not be described using current industry standards, such as the IEC 60909.

2.3 Short-circuits in Offshore Wind Power Plants

A short-circuit may be caused by natural accidents or failing equipment within the OWPP. During a short-circuit, the total impedance of the system is drastically reduced, causing high currents that may damage or degrade system equipment. Assume for instance that a 100 MW OWPP is operated at nominal power. In the event of a short-circuit, somewhere within the system, all power previously being transmitted at a controlled current level to the PCC will now rush towards the short-circuited node. Depending on the settings of various protection equipment in the system, the fault will be cleared within in a specific time period. Primarily transformers and breakers need to be designed and sized accordingly, in order to withstand the currents that may occur during the short-circuit time period, i.e. before the fault is cleared.

2.4 Low-Voltage-Ride-Through for Wind Power Generators

In the event of a three-phase line-to-ground short-circuit in an OWPP, the system voltage will decrease depending on the severity of the fault. By injecting a reactive current similar to VAR compensators, such as the SVC or STATCOM [33], the FRC WTG is able to support the grid during the fault by raising the system voltage. The LVRT capability of a FRC WTG describes the terminal voltage which the WTG is able to sustain during the time of the fault. In other words, the ability to ride through the fault. These capabilities have to fulfill the requirements stated by national grid codes. In figure 2.4 the LVRT requirements according to national grid codes in Germany, Great Britain (GB) and Denmark are illustrated. As can be seen in the figure, the minimum voltage requirement is increased as the duration of the fault is prolonged.

In addition to these requirements, the TSO might specify the amount of reactive current required for a given voltage drop at the WTG terminal. In figure 2.5, the minimum required reactive current defined by German E.ON is found. Voltage drops below 10 %, i.e. terminal voltages of 0.9 p.u. and above, are considered as the voltage dead band. For this voltage range, other sections of the E.ON grid code regulates the required behavior of the WTG [35]. Note that the values given in the figure are RMS values in p.u. and dictates an expected steady-state reactive current corresponding the voltage drop at the terminal. It is worth pointing out, however, that this steady-state current is quasi-stationary in the sense that the short-circuit current is assumed to behave stationary, for the limited time of the fault. During this time period, albeit short, the short-circuit current of the converter will still have plenty of time to stabilize to steady-state behavior. This can be seen in the dynamic simulations performed in [8, 9, 18].

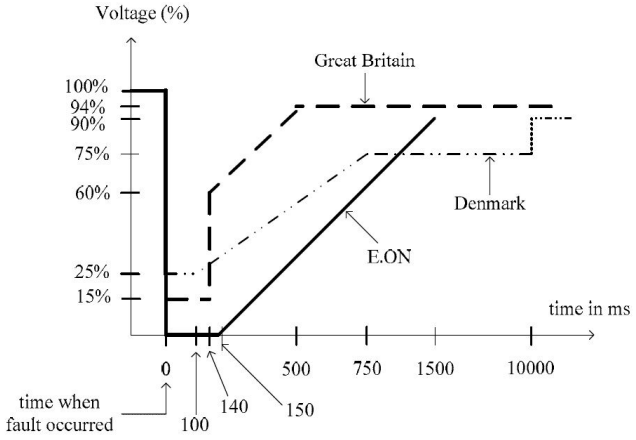

Figure 2.4. *LVRT requirements according to national grid codes in Germany, Great Britain and Denmark. Source: [34].*

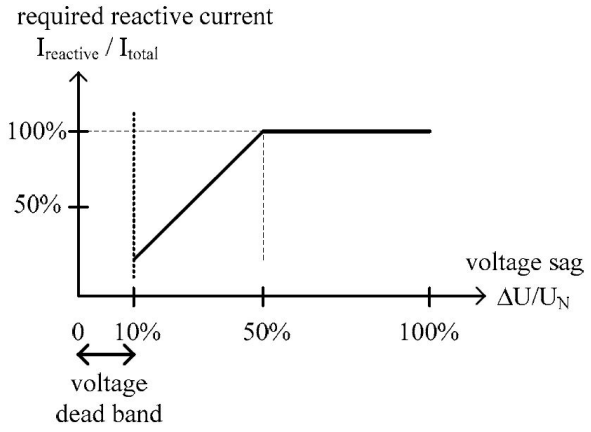

Figure 2.5. *E.ON grid code: Minimum required reactive current as a function of the terminal voltage drop. Source: [34].*

Chapter 3

Short-circuit Modeling

In this chapter, the static short-circuit calculation method performed by the industry standard IEC 60909 is instroduced, as well as the short-circuit calculations capabilities of DIgSILENT PowerFactory. Furthermore, the current source method developed for this project is presented, alongside a model for wind power plant aggregation.

3.1 IEC 60909

3.1.1 Introduction

International Electrotechnical Commission is an international organization promoting standards for use in industry and research. The IEC 60909 standard is used for calculations of short-circuit currents in three-phase AC systems [10]. The standard can be used both for low and high voltage systems up to 550 kV, with a system frequency of either 50 or 60 Hz. Both balanced and unbalanced faults are considered. The standard focuses on the calculation of maximum short-circuit current, as well as the minimum short-circuit current. The maximum short-circuit current dictates the capacity or rating of system components, while the minimum short-circuit current is used for determining the rating of fuses and other protection devices. For the purpose of this project, only the maximum short-circuit current is considered. The short-circuit calculations performed by the standard is based on the following general assumptions

- For the duration of the short-circuit, there is no change in the type of short-circuit involved, that is, a three-phase short-circuit remains three-phase and a line-to-earth short-circuit remains line-to-earth during the time of the short-circuit.

- For the duration of the short-circuit, there is no change in the network involved.

- The impedance of the transformers is referred to the tap-changer in main position. This is admissible, because the impedance correction factor K_T for network transformers is introduced.
- Arc resistances are not taken into consideration.
- All line capacitances and shunt admittances and non-rotating loads, except those of the zero-sequence system, are neglected.

The following sections will present a brief overview of selected parts of the standard relevant to this project.

3.1.2 Equivalent Impedance Modeling

The short-circuit calculations performed within the standard are based on an equivalent impedance representation of the electrical system under study. During a short-circuit, all considered components are replaced by their internal impedance, and an equivalent voltage source is applied at the fault node. This voltage source is the only driving force of the short-circuit current and all other sources are set to zero. Consider the electrical system in figure 3.1. Two non-rotating loads are connected to a network feeder through a 2-winding transformer with tap-changer. A three-phase fault occurs at the bus denoted F and the equivalent system found in figure 3.2 is obtained. The network feeder, transformer and transmission line are all represented by their internal impedances while the non-rotating loads are ignored. Note that the internal impedance of the network feeder is referred to the low-voltage side of the transformer. An equivalent voltage source $cU_n/\sqrt{3}$ is applied at the fault node, where U_n is the nominal bus voltage of that node. For the calculation of maximum short-circuit current, the voltage factor c_{max} defined in table 3.1, is to be used.

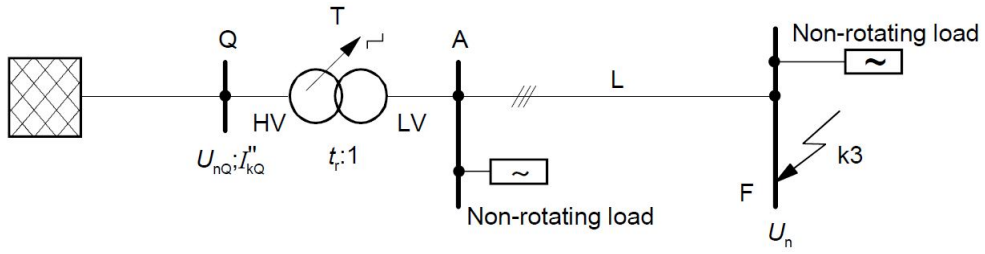

Figure 3.1. *Electrical test system. Source: [10].*

For the calculation of the maximum short-circuit current, the following conditions apply:

- In the absence of a national standard the voltage factor c_{max} should be used.
- Choose the system configuration and the maximum contribution from the power plants and network feeders which lead to the maximum value of the

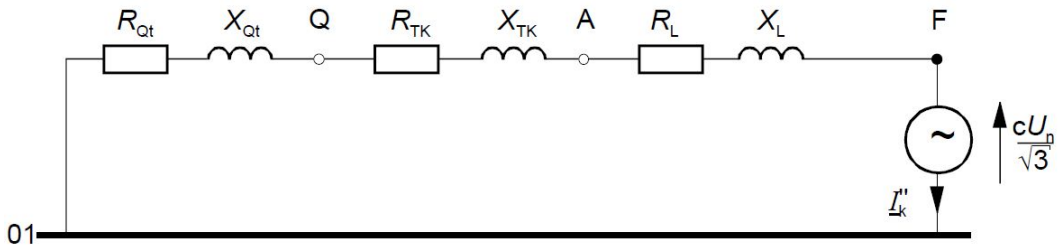

Figure 3.2. *Equivalent short-circuit impedance of the test system in figure 3.1. Source: [10].*

Table 3.1. *Voltage factor c_{max} used for the calculation of maximum short-circuit current.*

Nominal voltage, U_n	c_{max}
Low voltage, 100 - 1000 V (AC)	1.05
Medium voltage, 1000 V - 35 kV	1.10
High voltage, > 35 kV	1.10

short-circuit current at the short-circuit location, or for accepted sectioning of the network to control the short-circuit current.

- When equivalent impedances $\boldsymbol{Z_Q}$ are used to represent external networks, the minimum equivalent short-circuit impedance shall be used, which corresponds to the maximum short-circuit current contribution from the network feeder.
- Motors shall be included if appropriate, in accordance with Section 3.8 and 3.9 in [10].
- Resistance R_L of lines (overhead lines and cables) are to be introduced at a temperature of 20 °C.

For the calculation of balanced three-phase faults, only the positive sequence impedance of the network needs to be considered.

3.1.3 Impedance Models

Network feeder

The equivalent positive-sequence short-circuit impedance $\boldsymbol{Z_Q}$ of a network feeder is given by

$$Z_Q = \frac{cU_{n,Q}}{\sqrt{3}I''_{k,Q}}$$

where $U_{n,Q}$ is the nominal voltage at the connection of the network feeder and $I''_{k,Q}$ is the rated subtransient short-circuit current of the network feeder.
If the impedance ratio R_Q/X_Q is known, then the reactance X_Q can be determined from

$$X_Q = \frac{Z_Q}{\sqrt{1 + (R_Q/X_Q)^2}}$$

2-winding transformer

The short-circuit impedance Z_T of a two-winding transformer is given by

$$Z_T = \frac{u_{kr}}{100\%} \cdot \frac{U_{n,T}^2}{S_{n,T}}$$

where u_{kr} is the short-circuit voltage at rated current in per cent, $S_{n,T}$ is the rated power of the transformer and $U_{n,T}$ is the rated voltage of either the high or low voltage side. The real and imaginary part of Z_T are defined as

$$R_T = \frac{u_{Rr}}{100\%} \cdot \frac{U_{n,T}^2}{S_{n,T}}$$

and

$$X_T = \sqrt{Z_T^2 - R_T^2}$$

where u_{Rr} is the rated resistive component of the short-circuit voltage in per cent. In order to account for deviations caused by the tap-changer position of a transformer, an impedance correction factor K_T is introduced

$$K_T = 0.95 \frac{c_{max}}{1 + 0.6 x_T}$$

where x_T is the relative reactance of the transformer in Per Unit (p.u.). c_{max} should be determined from table 3.1 where U_n is the nominal voltage at the low-voltage terminal of the transformer.

3.1.4 Network types

When performing short-circuit calculations according to IEC 60909, the network topology as seen from the fault location will affect the choice of calculation procedure. There are two types of networks; meshed and radial or non-meshed. Essentially, these types distinguish between systems where the short-circuit currents from each source in the system are "mixed up" and divided in different branches, before reaching the short-circuit location. Each short-circuit branch, as seen from the short-circuit location will, in a radial network, contribute with a current originating from a single source. In the case of meshed network, the grid consists of one, or

more, parallel paths for the current to travel. The short-circuit current originating from one source will reach the short-circuit location through multiple branches. In general, one can assume that a large, complex power system consisting of multiple power corridors is meshed. A simpler, small-scale system will have to be analyzed more thoroughly according to the above criteria. For any larger OWPP, consisting of multiple WTG arrays, it is therefore safe to assume the system as meshed.

3.1.5 Short-circuit Currents

According to IEC 60909, the method used for the calculation of short-circuit currents should present the currents as a function of time for the full duration of the fault, corresponding to the instantaneous value of the voltage at the beginning of the short-circuit. The short-circuit current for a far-from-generator and near-to-generator short-circuit are illustrated in figure 3.3 and 3.4, respectively. Note how a far-from-generator fault is assumed to have a constant AC amplitude, while the near-to-generator fault has a decaying AC component. The current components found in figure 3.3 and 3.4 are briefly explained in table 3.2.

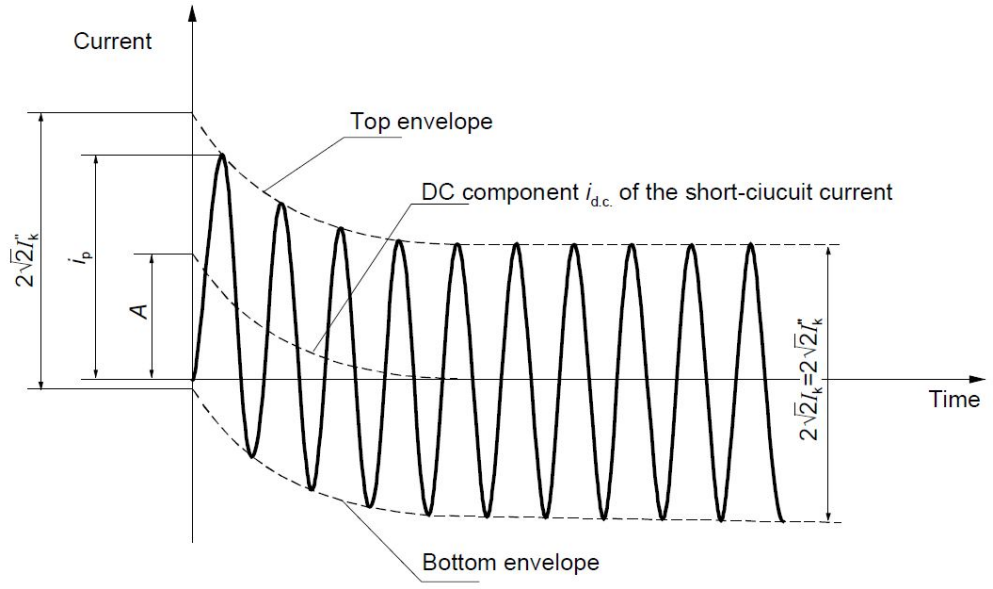

Figure 3.3. *Short-circuit current, far-from-generator.*

Subtransient short-circuit current

For a three-phase fault, the maximum subtransient short-circuit current $\boldsymbol{I''_k}$ can be calculated from

$$\boldsymbol{I''_k} = \frac{c_{max} U_n}{\sqrt{3}\boldsymbol{Z_k}}$$

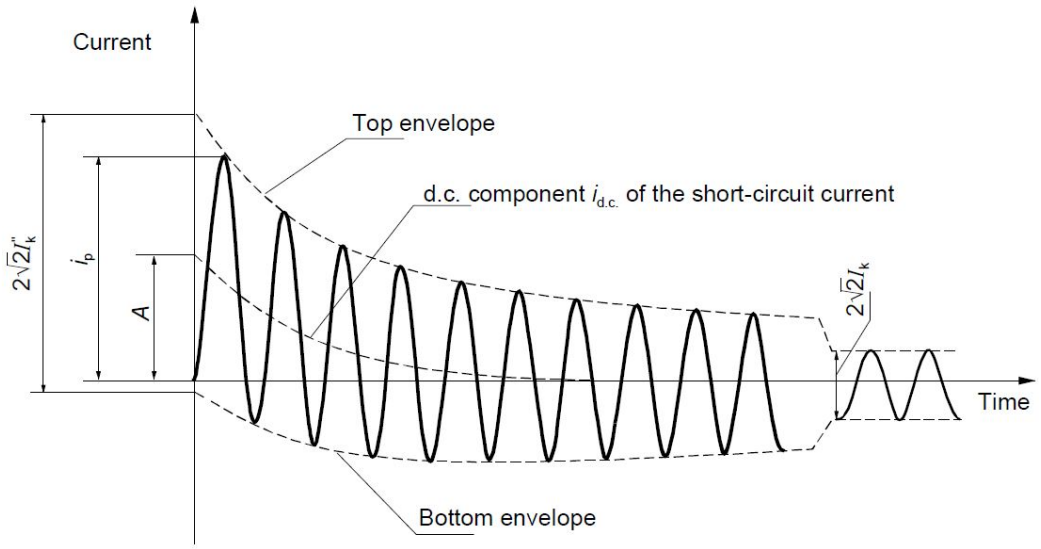

Figure 3.4. *Short-circuit current, near-to-generator.*

Table 3.2. *Brief explanations of short-circuit current components*

Component	Explanation
$\boldsymbol{I''_k}$	Initial or subtransient symmetrical short-circuit current
$\boldsymbol{I'_k}$	Transient short-circuit current
$\boldsymbol{I_k}$	Steady-state short-circuit current
i_p	Peak short-circuit current
$i_{d.c.}$	Decaying Direct Current (DC) component
A	Initial value of the DC component

where $\boldsymbol{Z_k}$ is the equivalent short-circuit impedance of the network. Consider the equivalent network illustrated in figure 3.2. The equivalent short-circuit impedance for this network would be $\boldsymbol{Z_k} = (R_{Qt} + R_{TK} + R_L) + j(X_{Qt} + X_{TK} + X_L)$. As mentioned earlier, the driving voltage of the short-circuit current is $c_{max}U_n/\sqrt{3}$.

Steady-state current

As can be seen in figure 3.3, the steady-state current of a far-from-generator fault can be assumed to be equal to the subtransient short-circuit current. For a fault near-to-generator, the symmetrical short-circuit current can be assumed to decay based on the type of generator, i.e. asynchronous or synchronous. For a meshed network with several sources it is, according to the standard, valid to make the following approximation for both near-to-generator and far-from-generator faults

$$\boldsymbol{I_k} = \boldsymbol{I_k''}$$

Peak current

The peak current in a radial network is defined as

$$\boldsymbol{i_p} = \kappa\sqrt{2}\boldsymbol{I_k''}$$

$$\kappa = 1.02 + 0.98\mathrm{e}^{-3R/X}$$

where R/X is the impedance ratio of the short-circuit impedance $\boldsymbol{Z_k}$.
For meshed networks, three calculation methods are proposed by the standard.

- *Method a*: For this method the lowest impedance ratio R/X of all branches connected to the fault location is considered for the calculation of κ.
- *Method b*: For this method the peak current is multiplied by a factor of 1.15, i.e. $\boldsymbol{i_p} = 1.15\kappa\sqrt{2}\boldsymbol{I_k''}$. If the impedance ratio R/X is below 0.3 in all connecting branches, the factor can be omitted. κ is determined using the impedance ratio of the reduced short-circuit impedance $\boldsymbol{Z_k}$ of the system. The product 1.15κ does not need to exceed 2.0 for high voltage networks and 1.8 for low voltage networks.
- *Method c*: For this method an equivalent impedance $\boldsymbol{Z_c}$ based on an equivalent system frequency f_c= 20 Hz for 50 Hz systems or f_c = 24 Hz for 60 Hz systems is utilized. The impedance ratio of $\boldsymbol{Z_c}$ is given from

  $$\frac{R_c}{X_c} = \frac{f}{f_c}\frac{R}{X}$$

  Here, the impedance ratio R_c/X_c is determined at low frequency. R/X is calculated according to the above equation and then used to determine κ. This method is recommended for meshed networks.

Decaying DC component

The decaying DC component of the short-circuit current is defined as

$$\boldsymbol{i_{d.c.}} = \sqrt{2}\boldsymbol{I_k''}\mathrm{e}^{-2\pi ftR/X}$$

where f is the system frequency and t is the time. If $t = 0$ the value of A in figure 3.3 and 3.4 is obtained. The impedance ratio R/X, should be calculated using *Method a*, or *c* described for the calculation of the peak current i_p. For meshed networks, *Method c* should be utilized, where the equivalent frequency f_c should be selected based on the product of the system frequency f and time t, see table 3.3.

Table 3.3. *Selection of f_c/f for Method c calculations of $i_{d.c.}$*

$f \cdot t$	< 1	< 2.5	< 5	< 12.5
f_c/f	0.27	0.15	0.092	0.055

Symmetrical breaking current

The symmetrical breaking current I_b, will depend on the network topology, i.e. meshed or radial, as well as the location of the fault, i.e. far-from-generator or near-to-generator. In this project, however, only meshed networks are considered. For such networks, the symmetrical current can be approximated as

$$\boldsymbol{I_b = I''_k}$$

for both far-from- and near-to-generator faults. By approximating the symmetrical current as the subtransient current, a conservative value is obtained.

Thermal equivalent current

The equivalent thermal current is an indication of the excess heat energy generated in the resistive elements of the system, caused by the short-circuit current. The thermal equivalent current is defined using the Joule integral

$$\int_0^{T_k} i^2 \mathrm{dt} = {I''_k}^2 (m+n) T_k = {I_{th}}^2 T_k$$

which results in

$$I_{th} = I''_k \sqrt{m+n}$$

The factors m and n are determined to account for the time-dependent heat effect of the decaying DC component and AC component, respectively. For a series of consecutive faults $i = 1, 2, 3, ..., N$, the thermal equivalent current is instead expressed as

$$\int i^2 \mathrm{dt} = \sum_{i=1}^{N} {I''_{k,i}}^2 (m_i + n_i) T_{k,i} = {I_{th}}^2 T_k$$

resulting in

$$I_{th} = \sqrt{\frac{\int i^2 \mathrm{dt}}{T_k}}$$

T_k is the total duration of each separate short-circuit duration $T_{k,i}$

$$T_k = \sum_{i=1}^{N} T_{k,i}$$

The DC dependent factor m can be calculated from

$$m = \frac{e^{4fT_k \ln(\kappa-1)} - 1}{2fT_k \ln(\kappa - 1)}$$

where κ should be selected according to the calculation method used for the calculation of $i_{d.c.}$. The factor n is dictated by the decay in the AC component. If $I''_k/I_k = 1$ then $n = 1$ and for $I''_k/I_k \neq 1$ the value of n is determined according to Annex A in [10].

3.2 DIgSILENT PowerFactory

3.2.1 Introduction

PowerFactory is a power system simulation tool developed by german DIgSILENT (Digital SimuLator for Electrical NeTwork), and can be used for a range of system studies, such as load-flow calculations, dynamic simulations, short-circuit calculations, harmonic studies etc. When performing steady-state simulations, a single-line diagram is representing the power system. Each system component is then modeled using a unique model including positive, negative and zero sequence impedances, load-flow characteristics and short-circuit behavior among many other options.

3.2.2 Short-circuit calculations

When performing steady-state short-circuit calculations in PowerFactory, there are a number of different calculation methods to choose from. The available methods are:

- IEC 60909 method.
- VDE 0102/0103 method.
- ANSI method, including IEEE C37 and 141 standards.
- Complete method.
- IEC 61363 method.

The short-circuit model used by each system component will be different, depending on the selection of calculation method. Furthermore, each method has a range of advanced calculation options available. There are, however, some basic input parameters common to all methods. These are listed below.

- Fault type - There are numerous available fault types, ranging from 3-phase to single phase including short-circuits, faults to neutral and neutral to ground. For the purpose of this project, only balanced 3-phase short-circuits have been considered.

- Fault impedance - The user has the option to select both the reactance X_f and resistance R_f of the fault itself. This impedance represents the shorted path caused by the fault. In addition to a standard representation of the fault impedance, there is an *enhanced fault impedance* option available, which takes the line-to-earth, as well as the line-to-line impedance into consideration. For the purpose of this project, only the standard representation of fault impedances have been considered.

- Fault location - The simulated fault can be placed at any terminal, busbar or along the length of any line in the system. In this project, only faults located directly at busbar or terminal connections have been considered.

3.2.3 Complete Method

When performing short-circuit calculations using the IEC 60909 standard, the state of the system prior to the fault is neglected. The voltage in each node is considered to be at its nominal value, while the operation or load-flow current is neglected. In addition to this, the voltage correction factor c is used to account for deviations from the real-life system and provide a conservative estimate. When performing simulations in a powerful software such as PowerFactory, the load-flow characteristics of the system prior to a fault can be easily obtained. The complete method used in PowerFactory is based on the same approach described within IEC 60909, i.e. a system description including the equivalent short-circuit impedance of each component, as well as an equivalent voltage source at the fault location (see Section 3.1). The equivalent voltage source is set to the pre-fault voltage of the fault node, and the calculated subtransient and transient short-circuit are superposed with the pre-fault operational current of the system. Furthermore, the use of the voltage correction factor c is optional and the transformer correction factor K_T is neglected. The results obtained through the complete method are less conservative, as compared with the IEC 60909 standard, while taking into account the pre-fault operational characteristics of the system.

In addition to taking more system data into consideration, as compared with the IEC 60909 standard, the complete method also includes the short-circuit behavior for basic components such as the AC voltage source used in [21], and the AC current source, used in the method developed for this project. In the implementation of the IEC 60909 method in PowerFactory, both sources mentioned above are simply left open circuit. When developing a method in PowerFactory which allows for manipulation of the short-circuit behavior, the use of the complete method is therefore necessary.

Besides determining the steady-state short-circuit current, this project also aims to find other relevant current quantities. As mentioned previously, these are the decaying DC component $i_{d.c.}$, the symmetrical breaking current I_b and the ther-

mal equivalent current I_{th}. The calculation methods available in PowerFactory for determining these quantities are based on the IEC 60909 standard. These methods are briefly described below. Note that the methods described in IEC 60909 are written with a lower case letter, while the implemented calculation methods in PowerFactory are written with an upper case letter.

- *Method B* - With this option the calculation of κ, as well as $i_{d.c.}$, are calculated according to *method b*, as described in the IEC 60909 standard. Note that only *method a* and *c* are recommended in IEC 60909 for the calculation of $i_{d.c.}$. *Method B* will therefore base the impedance ratio used in the expression for $i_{d.c.}$ on the network reduction impedance, as well as adding an extra factor of 1.15 to the expression.

- *Method C(1)* - Similar to the above option, this enables the use of *method c* as described by IEC 60909 for the calculation of κ and $i_{d.c.}$. The equivalent impedance is calculated according to table 3.3.

- *Method C(012)* - Identical to *Method C(1)*, but also takes the impedance of each sequence into consideration.

For this project, *Method C(1)* is used based on the recommendations stated by IEC 60909, when dealing with meshed systems. It has been discovered, through simulations and post-calculations, that the impedance ratio R/X of the reduced network impedance $\boldsymbol{Z_k}$, in all above methods will be calculated based on system representation where AC voltage and current sources are left open circuit.

3.3 Current Source Method

3.3.1 Introduction

In order to obtain the expected short-circuit contribution from each FRC WTG, a new iterative method was developed for the purpose of this project. The method is designed and implemented in PowerFactory, and is based on the AC current source model available within the software. In the following sections, the method algorithm will be described in greater detail. First, the method is described in general along with a description of the current source model and the implementation of the grid code voltage control curve. Secondly, the iterative algorithm implemented in PowerFactory is described in greater detail.

3.3.2 Method Description

Current Source Model

The AC current source model used in PowerFactory has three basic parameters

- I_n: Rated current of the source in kA.
- i_{cap}: Sets the source as capacative ($i_{cap} = 1$) or inductive ($i_{cap} = 0$).
- i_{setp}: RMS value of the output current in p.u.. or the current set point of the source.
- $\cos\phi$: Power factor of the source.

In order to obtain a short-circuit current based on an arbitrary reference value, the source parameters need to be altered iteratively, much like what is described in [21]. For this method, the current set point will be set to the specified maximum total current during a short-circuit, i.e. $i_{setp} = i_{max}$. This is a conservative assumption, considering that the WTG does not necessarily need to output maximum current during a short-circuit. In order to obtain a worst-case scenario, however, this is assumed to be the case. Note that while this is the case for the total current, the reactive and active current components are determined from the reference curve described later in this section.

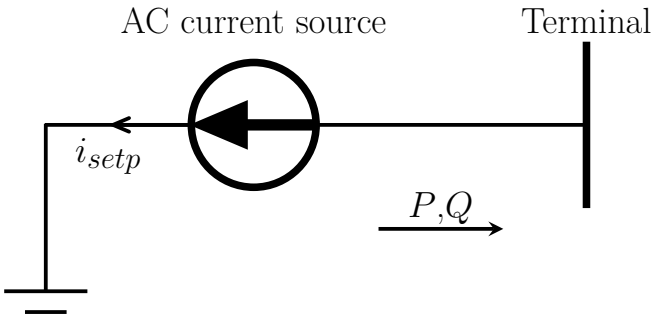

Figure 3.5. *PowerFactory current source model*

The above parameters will dictate the steady-state behavior of the source for load-flow simulations. Ideally, the output of the source would be unchanged during a short-circuit. This, however, is not the case when using the complete method in PowerFactory, since the load-flow characteristics of a component will affect its short-circuit model. Consider the following example; for a specific voltage drop at the source terminal the current source needs to provide a short-circuit current, corresponding to the reference values $i_{q,ref}$ and $i_{d,ref}$. These will be explained in greater detail in the next section. Through an iterative process, the values of i_{cap}, i_{setp} and $\cos\phi$ are altered such that the correct reference values are obtained, resulting in $i_{cap} = 0$, $i_{setp} > 0$ and $0 \leq \cos\phi \leq 1$. Note that the load-flow behavior of the current source for these parameters is inductive. The resulting short-circuit behavior, however, would for this example be capacative. This is because of the difference in the load-flow model and short-circuit model used in the complete method. It is

worth pointing out, that the RMS value of the total short-circuit current will correspond to i_{setp}. In figure 3.5, the principal operation of the current source model in PowerFactory is depicted. The current direction is defined from the terminal to ground.

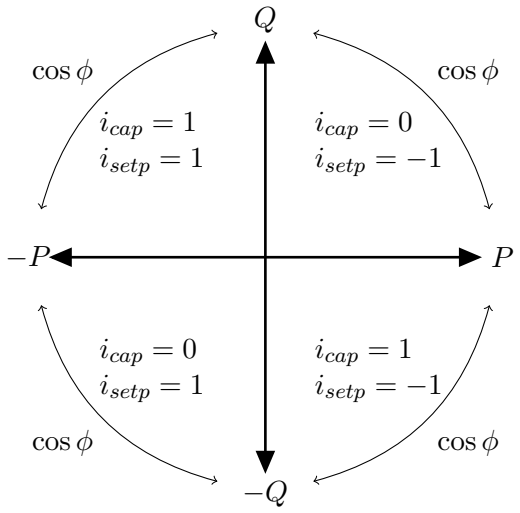

Figure 3.6. *PowerFactory current source model*

The power flow direction defined in figure 3.5 is related to the values of i_{cap}, i_{setp} and $\cos\phi$. In figure 3.6, the four current quadrants and the coupled power flow directions, are defined as a function of i_{cap}, i_{setp} and $\cos\phi$. During normal operations, for instance, the current source need to operate in the first quadrant in order to provide active and reactive current to the grid. Here, $\cos\phi = 1$ corresponds to full active power generation or absorption, and $\cos\phi = 0$ full reactive generation or absorption. For a specific short-circuit, however, the model may need to be operated in any of the four quadrants, in order to obtain the specified reference values. In the iterative process of converging to a solution, this four quadrant representation of the current source has been used. One downside of this representation is that the short-circuit current is not clearly defined for fixed values of i_{cap}, i_{setp} and $\cos\phi$. Most notable is that $\cos\phi = 1$ and $\cos\phi = 0$ not necessarily will correspond to a minimum or maximum reactive power generation, during the short-circuit. This will mainly depend on the load-flow results of the rest of the system and is an effect of the superposition of currents used in the complete method. In other words, the parameters used to control the source are coupled with the load-flow behavior and is only partly correlated with the short-circuit behavior.

Grid Code Voltage Control Curve

Consider the reference reactive current according to the voltage control curve in figure 3.7. The current source method is implemented based on the assumption that the regulation curve provided by a TSO is of the same canonical form. An example of such a curve can be found in figure 2.5. Here, Δu is the voltage drop or retained voltage at the WTG terminal, i.e. the terminal in figure 3.5. The grid code can be divided into three regions:

- $0 \leq \Delta u < u_{DB}$: For voltage drops below the dead band voltage u_{DB}, the turbine generator is assumed to output the rated active current, i.e. $i_{setp} = \pm 1.0$ depending on the current quadrant. In other words $i_{q,ref} = 0$ and $i_{d,ref} = 1.0$.
- $u_{DB} \leq \Delta u < i_{q,max}/K$: For voltage drops above u_{DB}, the turbine generator is required to provide a minimum reactive current according to the linear curve $i_{q,ref} = K\Delta u$. Note that this is a minimum requirement, and that some manufacturers will, depending on the controller used for the converter, provide more reactive current than what is required by the grid code. In such cases, a specific value $i_{q,min} \neq 0 \leq i_{q,max}$ can be used for the voltage range $u_{DB} \leq \Delta u$, see figure 3.7. The reactive current component is assumed to be prioritized. Therefore the active current reference $i_{d,ref}$ is determined by the slack of the maximum total current and the specified maximum active current, i.e. $i_{d,ref} = \sqrt{{i_{max}}^2 - {i_{q,ref}}^2} \leq i_{d,max}$.
- $i_{q,max}/K \leq \Delta u$: For a certain terminal voltage, the turbine is required to output its maximum reactive current, i.e. $i_{q,ref} = i_{q,max}$. Similar to the above region, the active current reference is determined by the slack of the total current i_{max}.

For over-voltages at the turbine terminal, i.e. $\Delta u < 0$, the reactive current component is assumed to be zero, while the active current is assumed to be at its maximum. In reality, the converter would act differently, e.g. absorb reactive power to lower the voltage at the terminal. This behavior is, however, not considered for this project, based on the assumption that the resulting terminal voltage for all generators in the system will drop during a short-circuit.

Smoothing Function

Consider the grid code implementation in figure 3.7. When the method attempts to converge to a reference value at the boundary of the dead band voltage, it might be forced into a state of non-convergence. This is caused by the rapid change of reference values, as the measured voltage is either slightly above the dead band, or below. In order for the iterative method to converge for the discontinuity at Δu_{DB}, the following polynomial smoothing function is introduced. Let the reactive component of the smoothing function be

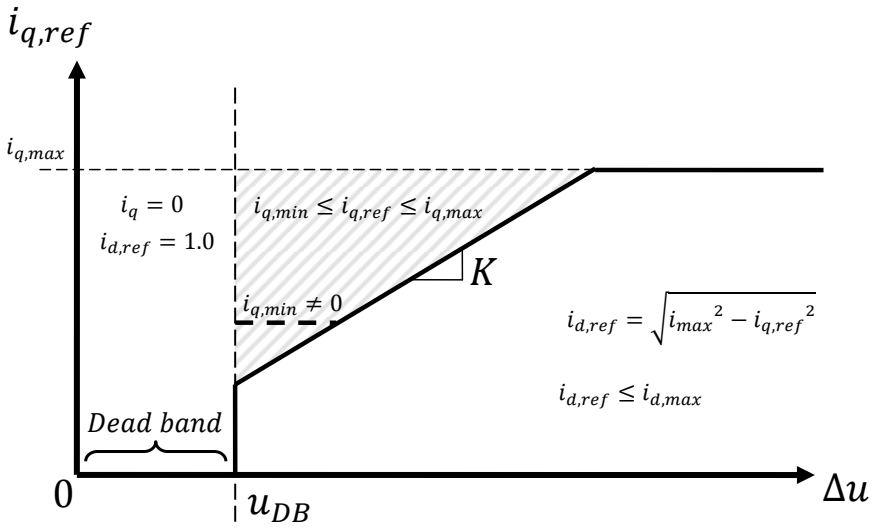

Figure 3.7. *Grid code regulation used for the current source method.*

$$f_q(\Delta u) = \left(\frac{\Delta u}{c_q}\right)^n$$

where n is the polynomial factor and c_q a scaling constant to be determined. The boundary conditions of the smoothing function are

$$f_q(0) = 0 \quad \text{and} \quad f_q(u_{DB}) = i_q(u_{DB}) = K \cdot u_{DB}$$

From the second condition c_q can be determined

$$\left(\frac{u_{DB}}{c_q}\right)^n = K \cdot u_{DB} \implies c_q = \frac{u_{DB}}{(K \cdot u_{DB})^{1/n}}$$

The real part of the smoothing function is derived from the maximum allowed active current component within the dead band.

$$f_d(\Delta u) = \begin{cases} 1.0 - \left(\frac{\Delta u}{c_d}\right)^n & \text{if } \sqrt{i_{max}^2 - i_q(u_{DB})^2} > 1.0 \\ 1.0 + \left(\frac{\Delta u}{c_d}\right)^n & \text{if } \sqrt{i_{max}^2 - i_q(u_{DB})^2} \leq 1.0 \end{cases}$$

Assuming that the converter is providing its maximum total current, the following boundary conditions are obtained

$$f_d(0) = 1.0 \quad \text{and} \quad f_d(u_{DB}) = \sqrt{i_{max}^2 - i_q(u_{DB})^2} = \sqrt{i_{max}^2 - \left(K \cdot u_{DB}\right)^2}$$

where the scaling factor c_d can be determined from the second condition

$$1.0 \pm \left(\frac{u_{DB}}{c_d}\right)^n = \sqrt{i_{max}^2 - (K \cdot u_{DB})^2} \implies c_d = \frac{u_{DB}}{\left|1.0 - \sqrt{i_{max}^2 - \left(K \cdot u_{DB}\right)^2}\right|^{1/n}}$$

In figure 3.8(a) and 3.8(b) the smoothing function for the reactive and active component, respectively, are plotted for $n = 10, 50, 100$. For these figures, the current limits were set to $i_{max} = i_{d,max} = i_{q,max} = 1.0$ and $i_{q,min} = 0$. Note that the value of $i_{q,min}$ at u_{DB} will affect the choice of n. In order to avoid non-convergence at the discontinuity, the value of n should be decreased as $i_{q,min}$ is increased. This is due to the fact that a high value of n will cause the reference curve to become to steep as the gap between $i_{q,ref} = 0$ and $i_{q,ref} = i_{q,min}$ grows larger.

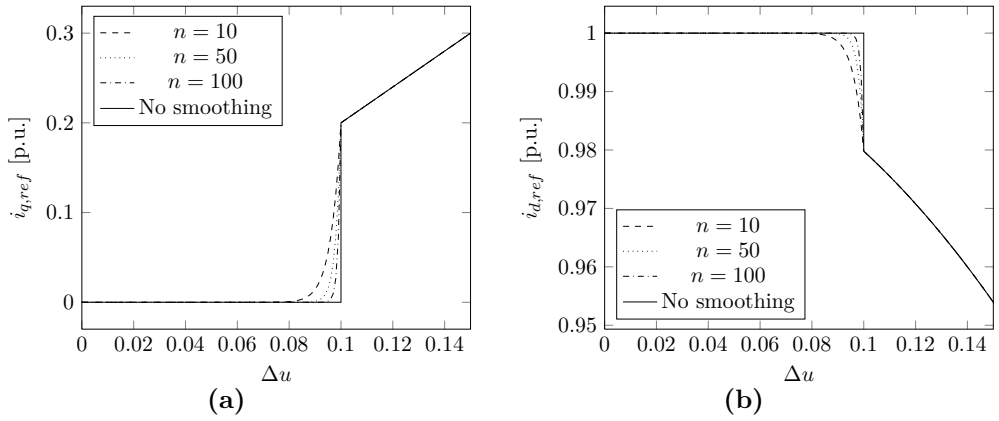

Figure 3.8. *Smoothing function for the active component,* $n = 10, 50, 100$.

Deviation factor δ

When treating the resulting short-circuit current I_k in the bus bar, three different calculation errors caused by short-comings of the method need to be taken into consideration. These errors are:

- The inherit error caused by the absolute power angle error threshold allowed by the iterative current source method.

- Power angle deviations, occurring when current sources are electrically separated by bolted, or almost zero impedance faults. For this type of faults, the current sources are "maxed out" or saturated, without being able to provide a purely reactive current, with the exception of bolted faults at the current source terminal. This phenomenon also occurs for some rare cases when the voltage drop is close to 1 p.u..

- Errors introduced by the smoothing function. Since the source will adjust according to values set by the smoothing function there will be a deviation from the expected reference value, which in this case, is zero.

In order to evaluate the impact of these errors on the total short-circuit current at the fault location, the deviation factor δ is introduced. In the case of complete convergence of each source, i.e. within the allowed error threshold, the error of each source will be negligible. Assume instead that each source fails to provide the specified reference value and deviates by a considerable amount. Simply looking at the absolute error for each source will not provide a good measurement of the accuracy of the total short-circuit current obtained in the simulation. The error introduced by each source needs to be evaluated based on its relative effect on the total short-circuit current, to be able to make any claims about the accuracy of the method. Consider an OWPP consisting of several FRC WTGs. Assume that each source converges with an absolute error of 5 % for a specific short-circuit case, and that the short-circuit contribution from the grid is many times larger than that of the turbines. Simply stating that the error of the simulation is 5 % would be inaccurate, but should rather be scaled according to its effect on the total short-circuit. For instance, if the grid is very strong, while the turbines are few and of low power rating, an error of 5 % would be negligible.

Consider the resulting short-circuit current I_{k,CS_i} of each current source $i = 1, 2, \ldots, N$. The error factor of each current ξ_i is evaluated according to

$$\xi_i = |\mathrm{e}^{j\phi_i} - \mathrm{e}^{j\phi^*_{ref,i}}| = \sqrt{(\cos(\phi_i) - \cos(\phi^*_{ref,i}))^2 + (\sin(\phi_i) - \sin(\phi^*_{ref,i}))^2}$$

Here, ϕ_i is the power angle of source i obtained through simulations while $\phi^*_{ref,i}$ is the reference value calculated by neglecting the smoothing function. The error factor provides a way of scaling the short-circuit current of each source to the non-linear deviation caused by the error.

Assuming that the external feeding network is contributing with a major part of the short-circuit current, and that this current is more or less unaffected by the currents provided from the turbines (this will be true in the case of bolted faults), the deviation factor δ is given by

$$\delta = \frac{\sum_{i=1}^{N} I_{k,CS_i}(\frac{U_{n,CS_i}}{U_{n,k}})\xi_i}{\sum_{j=1}^{M} I_{k,Q_j}(\frac{U_{n,Q_j}}{U_{n,k}})} \tag{3.1}$$

The respective current is referred to the nominal voltage level $U_{n,k}$ of the short-circuited bus bar or terminal. The denominator is the sum of each short-circuit current I_{k,Q_j} provided by any feeding network $j = 1, 2, \ldots, M$. $U_{n,CS}$ and $U_{n,Q}$ denotes the nominal voltage level of the current source, and external network feeder,

respectively. The error factor introduced in the above expression provides a variable estimate of the deviation from the true or expected result. Consider, once again, the case when there is complete convergence in the method. If the error factor was not used to scale the source currents, the obtained deviation would not reflect the fact that the method has arrived at an expected value, but would rather provide a relationship between the total current from the grid and the turbines.

Current calculations

The relevant simulation results obtained in PowerFactory and used by the method are I'_k, $i_{d.c.}$, I_b and I_{th}. Here, the transient short-circuit current I'_k is equal to the steady-state short-circuit current I_k. I'_k is the total short-circuit current in the bus bar or terminal. The values of $i_{d.c.}$, I_b and I_{th} are all calculated according to the selected calculation method in the complete method, see Section 3.2, and based on the value of I'_k. This is due to the fact that both the transient and subtransient short-circuit from the grid and current sources are identical. The short-circuit models used for the external grid, and current source, are based on subtransient values, which will be identical to the transient and steady-state values, given that the system is meshed. Based on the recommendations in IEC 60909, *Method C(1)* has been used for this project. Note, that for the calculation of impedance ratio of the grid, the current sources are left open circuit. The DC component of the short-circuit contribution from each WTG can therefore be viewed as ignored. This is consistent with the fast transient response of the FRC WTG controller. If one studies the simulated transient response of different types of FRC WTGs in [8, 9, 18], the DC component is seemingly close to zero. Similarly, the thermal equivalent current is also calculated based on the exclusion of DC contribution from the current sources.

The deviation factor δ derived in the previous section is used for post-calculation of an conservative estimate of the resulting short-circuit current I'_k. This post-calculation is carried out according to

$$I'_{k,\delta} = I'_k(1 + 2\delta)$$

This value is conservative, in the sense that the original current I'_k, is increased two times the deviation factor. This is to account for the worst case scenario, when the error in the current source currents completely cancels out a portion of the total short-circuit current. The purpose of this value is to provide an estimate of the true short-circuit current that would have been obtained, given that all sources converged completely, while at the same time providing a certain level of conservativeness.

3.3.3 Iterative Algorithm

The iterative algorithm implemented in PowerFactory is based on an outer and inner loop, see figure 3.9. The outer loop iterates through all available current sources in

the system and passes them to the inner loop one by one. This process is repeated, until all current sources have converged within one single iteration of the outer loop, or the maximum number of iterations have been reached. The inner loop iteratively alters the current source parameters according to the reference values defined by the terminal voltage drop at each source. The loop is terminated either when the current source has converged to the reference values, the maximum number of inner loop iterations have been reached or the source has saturated. At the end of the algorithm relevant values are calculated or obtained from simulation results. In table 3.4, the basic input parameters required by the algorithm, can be found.

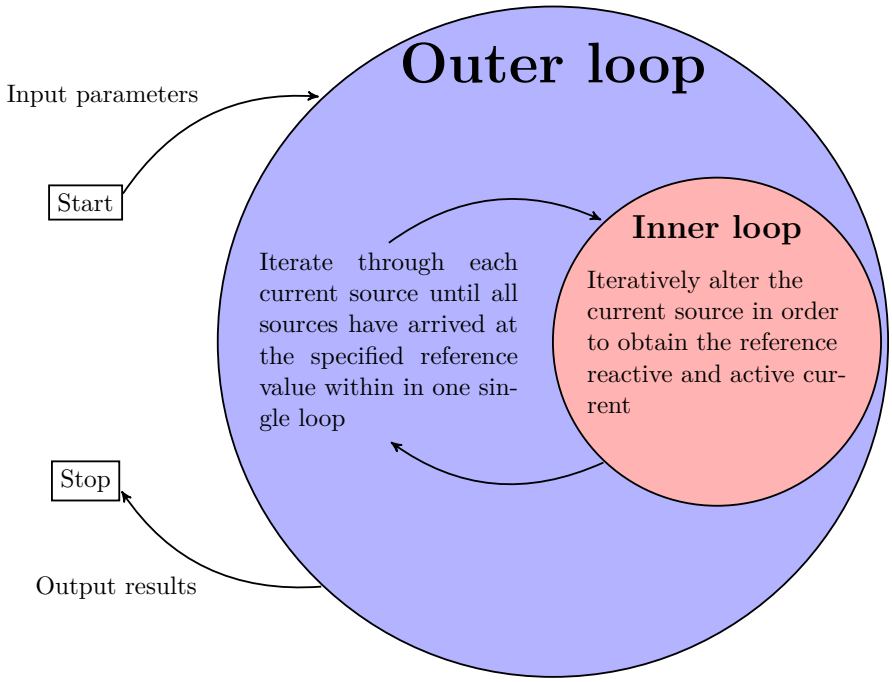

Figure 3.9. *PowerFactory current source model.*

Note that the iterative algorithm only serves to determine the steady-state short-circuit contribution of each turbine, as well as calculating the deviation factor δ. All other relevant quantities are obtained from PowerFactory simulation results and post-processed values based thereof. In the following paragraphs, the inner and outer loop algorithm are explained in more detail, using algorithm flow charts. In figure 3.10, a description of the blocks used in this type of representation can be found.

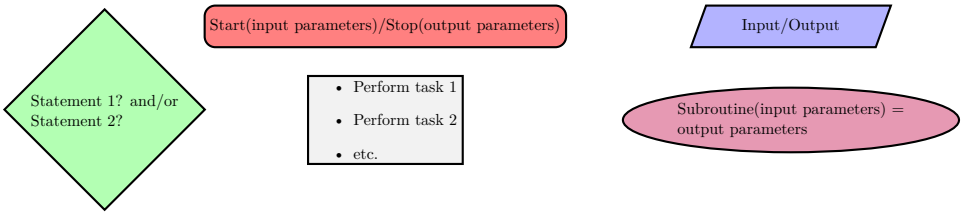

Figure 3.10. *Explanation of algorithm flow chart building blocks.*

Table 3.4. *Basic input parameters required by the iterative algorithm.*

Parameter	Description
i_{max}	Maximum total output current of the FRC WTG in p.u. during a short-circuit.
$i_{q,max}$	Maximum reactive current of the FRC WTG in p.u. during a short-circuit.
$i_{q,min}$	*Optional.* Minimum reactive current of the FRC WTG in p.u. during a short-circuit. If this value is not specified, i.e. set to zero, then $i_{q,min} = k\Delta u$.
$i_{d,max}$	Maximum active current of the FRC WTG in p.u. during a short-circuit.
$nIter1$	Maximum allowed number of iterations for the outer loop. Default value: 100
i_{cap}	Initial current type setting of each current source. Default value: 1
i_{setp}	Initial current direction of each current source. Default value: -1.0
$\cos\phi$	Initial power factor of each current source. Default value: 0.1
ϕ_{err}	Absolute power angle error tolerance used in the inner loop. Recommended value: 0.05°
$nIter2$	Maximum allowed number of iterations for the inner loop. Default value: 10
k_n	Nudge factor used in the inner loop. Can be increased to improve convergence times, or decreased in the rare event of rapid changes of reference values at the dead band voltage. Default value: 1.0.
u_{DB}	The dead band voltage is the retained voltage in p.u. at the WTG terminal at the point where the reactive current output of the turbine generator should be controlled according to the assumed grid code voltage control curve.
K	Slope of the linear control region of the grid code voltage control curve.
n	Polynominal factor of the smoothing function. Should be decreased if the algorithm has difficulties converging for $i_{q,min} \neq 0$. Default value: 100

Inner loop

Consider the inner loop flow chart in figure 3.11. The algorithm is initialized by running a short-circuit calculation and setting the counters $iResOk$ and $iMaxedOut$ to zero. From the initial short-circuit calculation, the bus voltage at the current source terminal is measured, as well as the power angle ϕ. Note that settings for the short-circuit calculation, such as the fault location and fault impedance, need to be setup externally in PowerFactory under the "Short-circuit calculation"-tab. From the initial short-circuit calculation, the initial reference currents are determined by the subroutine $RefCurrents$. This subroutine is implemented based on the grid code reference curve and smoothing function described in Section 3.3.2.

The resulting reference active and reactive current are used to calculate the reference power angle ϕ_{ref}. Note the minus sign appearing in the expression found in figure 3.11. The desired current fed into the grid should be inductive, i.e. the reactive current should be lagging the active component. Furthermore, the current set point is scaled according to the total reference current. At this point, the absolute error between the actual and reference power angle is determined. If it is below the threshold value $\phi_{err} = |\phi - \phi_{ref}|$, the current parameter settings of the source is acceptable and the loop sets $iResOk = 1$ before it is terminated. When developing this method, the error threshold was set to $\phi_{err} = 0.05°$, which also is the recommended value. This value was selected since it provided sufficiently accurate results, while not impeding the convergence of the method.

If the actual power angle is outside of bounds, i.e. the error threshold, the loop will start altering the parameters of the source iteratively. The rate at which the power angle of the source is altered is determined by $k_i = 1 + k$ and $k_d = 1 - k$, where k is the alteration coefficient. Depending on the actual and reference power angle, as well as the power factor of the source, k will be set according to table 3.5. As can be seen in the table, k is determined by a constant part multiplied with the absolute difference in power angle and reference power angle $|\phi - \phi_{ref}|$. The constant part has been determined through an iterative process, where the values were set in order to obtain convergence in a large amount of operation scenarios. In general, it can be noted that when the source is operated close to unity power factor $\cos\phi = 1$, the rate at which the source should be altered is reduced. The relative factor $|\phi - \phi_{ref}|$ helps to speed up the iteration by increasing k when the error is large, and reducing it when the method is very close to a solution.

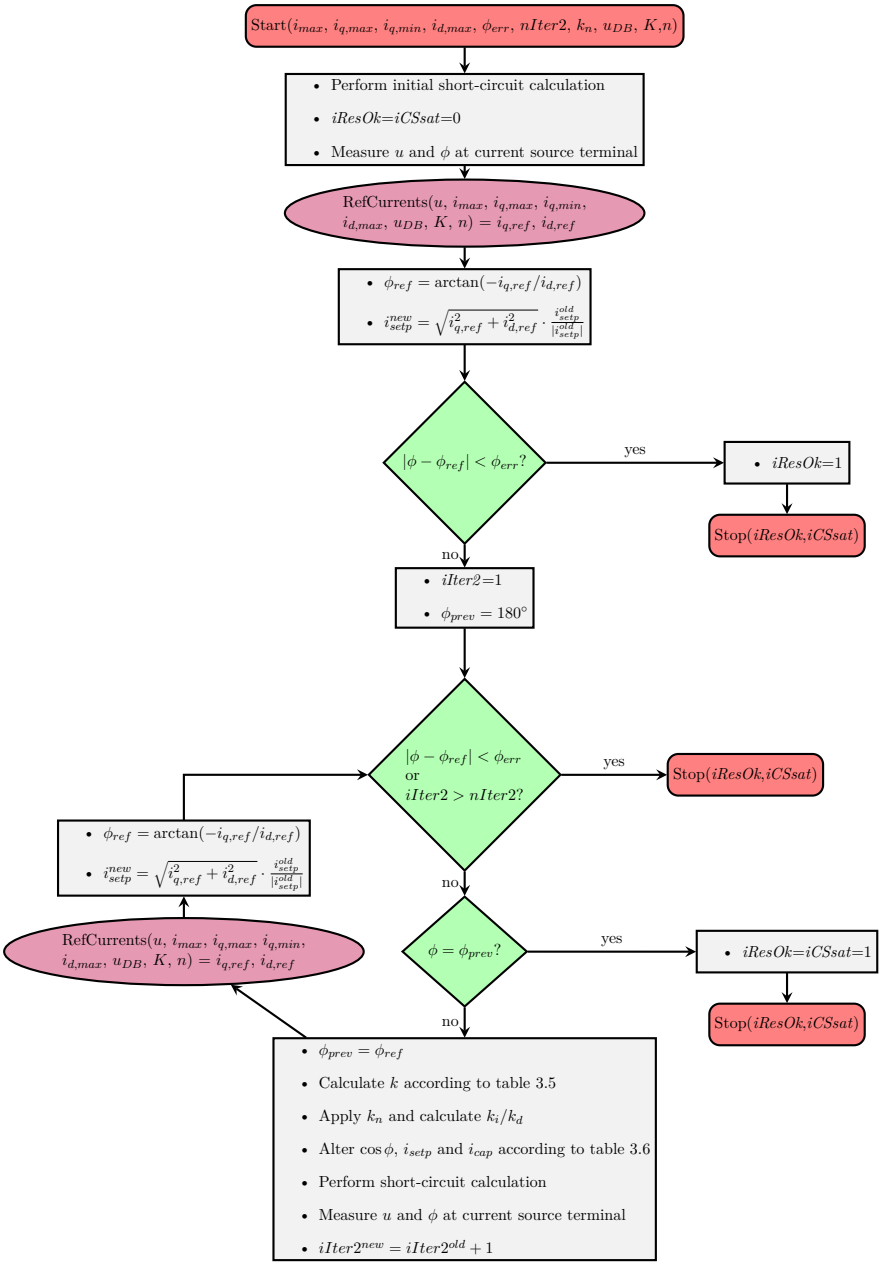

Figure 3.11. *Inner loop*

Table 3.5. *Alteration coefficient k*

$\lvert\phi - \phi_{ref}\rvert$	$\lvert\phi\rvert$	$\cos\phi$	k
$> 45°$			$0.025 \cdot \lvert\phi - \phi_{ref}\rvert$
$> 30°$			$0.0025 \cdot \lvert\phi - \phi_{ref}\rvert$
$> 5°$	$< 60°$	> 0.97	$0.0001 \cdot \lvert\phi - \phi_{ref}\rvert$
		< 0.97	$0.001 \cdot \lvert\phi - \phi_{ref}\rvert$
	$> 60°$		$0.025 \cdot \lvert\phi - \phi_{ref}\rvert$
$> 1°$	$< 60°$	> 0.97	$0.00005 \cdot \lvert\phi - \phi_{ref}\rvert$
		< 0.97	$0.001 \cdot \lvert\phi - \phi_{ref}\rvert$
	$> 60°$		$0.025 \cdot \lvert\phi - \phi_{ref}\rvert$
$< 1°$	$< 60°$	> 0.97	$0.00002 \cdot \lvert\phi - \phi_{ref}\rvert$
		< 0.97	$0.005 \cdot \lvert\phi - \phi_{ref}\rvert$
	$> 60°$		$0.025 \cdot \lvert\phi - \phi_{ref}\rvert$

Depending on the difference in power angle, and the quadrant in which the current source is operating, the current source parameters need to be set according to table 3.6. These regions are implemented based on the current quadrants found in figure 3.6. The column labeled "Action" provides information regarding what changes are made to the current source parameters. These will depend on the conditions listed in the remaining columns and rows in the table. The subscript *old* indicates the current value of the parameter, while *new* is the new value, calculated based on the old one. The variable ϕ_{prev} is used to keep track of the cases when the reactive current of the source is saturated. At this point, the source parameters are changed, but has no effect on the resulting short-circuit current (this is a consequence of using the Complete Method in PowerFactory). For this case, $iResOk = 1$ and $iCSsat = 1$ before the loop is terminated. When the source is set to a new quadrant, the parameter ϕ_{prev} is set to $-180°$. This is because the behavior of the source will be unchanged at the boundary between two quadrants.

There are two special cases implemented in the inner loop when determining how the source should be altered. The first one is when $k_i \cos\phi_{old} > 1$. This corresponds to the case when an increase in the power factor parameter would be outside of the allowed bounds of the current source model. To amend this, $\cos\phi$ is simply set to 1. The other case is when $k_d \cos\phi_{old} < 0.001$. In this case, the reduction of the current value of $\cos\phi$ will be too small to make any change, and it is simply set to 0. Also, it is worth pointing out that the method only allows the source to move from the first quadrant to the fourth, and vice verse. During the implementation of the method, it was discovered that there was no need to allow the source to move in any other direction when operating in these quadrants.

Table 3.6. *Adjustment of the current source. The action taken to alter the source depends on the current quadrant in which the source is currently operating, as well as the actual power angle and power factor.*

Quadrant	i_{cap}	i_{setp}	ϕ	$\cos\phi$	Action
1st	0	< 0	$< \phi_{ref}$	0	$\cos\phi_{new} = 0.01$
				1	Change to 4th quadrant: $i_{cap} = 1$ $\phi_{prev} = -180°$
				-	$k_i \cos\phi_{old} > 1 \Rightarrow \cos\phi_{new} = 1$ $k_i \cos\phi_{old} \leq 1 \Rightarrow \cos\phi_{new} = k_i \cos\phi_{old}$
			$> \phi_{ref}$	-	$\cos\phi_{new} = k_d \cos\phi_{old}$
2nd	1	> 0	$< \phi_{ref}$	0	Change to 1st quadrant: $i_{cap} = 0$ $\phi_{prev} = -180°$ $i_{max} = -1$
				-	$k_d \cos\phi^{old} < 0.001 \Rightarrow \cos\phi_{new} = 0$ $k_d \cos\phi^{old} \geq 0.001 \Rightarrow \cos\phi_{new} = k_d \cos\phi_{old}$
			$> \phi_{ref}$	1	Change to 3rd quadrant: $i_{cap} = 0$ $\phi_{prev} = -180°$
				-	$k_i \cos\phi_{old} > 1 \Rightarrow \cos\phi_{new} = 1$ $k_i \cos\phi_{old} \leq 1 \Rightarrow \cos\phi_{new} = k_i \cos\phi_{old}$
3rd	0	> 0	$< \phi_{ref}$	1	Change to 2nd quadrant: $i_{cap} = 1$ $\phi_{prev} = -180°$
				-	$k_d \cos\phi_{old} < 0.001 \Rightarrow \cos\phi_{new} = 0$ $k_d \cos\phi_{old} \geq 0.001 \Rightarrow \cos\phi_{new} = k_d \cos\phi_{old}$
			$> \phi_{ref}$	0	Change to 4th quadrant: $i_{cap} = 1$ $\phi_{prev} = -180°$ $i_{setp} = -i_{max}$
				-	$k_i \cos\phi_{old} > 1 \Rightarrow \cos\phi_{new} = 1$ $k_i \cos\phi_{old} \leq 1 \Rightarrow \cos\phi_{new} = k_i \cos\phi_{old}$
4th	1	< 0	$< \phi_{ref}$	-	$k_d \cos\phi_{old} < 0.001 \Rightarrow \cos\phi_{new} = 0$ $k_d \cos\phi_{old} \geq 0.001 \Rightarrow \cos\phi_{new} = k_d \cos\phi_{old}$
			$> \phi_{ref}$	1	Change to 1st quadrant: $i_{cap} = 0$ $\phi_{prev} = -180°$
				-	$k_i \cos\phi_{old} > 1 \Rightarrow \cos\phi_{new} = 1$ $k_i \cos\phi_{old} \leq 1 \Rightarrow \cos\phi_{new} = k_i \cos\phi_{old}$

Outer loop

Consider the outer loop flow chart in figure 3.12. The method is initialized by setting all current sources according to input, i.e. i_{cap}, i_{setp} and $\cos\phi$. Note that the current set point i_{setp} will be scaled by the input parameter i_{max} for all sources. The recommended values of i_{cap}, i_{setp} and $\cos\phi$ are found in table 3.4, and were used in the development of this method. In each iteration of the outer loop, an attempt to converge to the reference value of each source is made using the inner loop. If a source is within the tolerance ϕ_{err} at the start of the inner loop, or if it is saturated, the source will be flagged as acceptable, i.e. $iResOk = 1$. If all sources are considered as acceptable within one single loop of the iteration, the method is considered as completed. At this point, the deviation factor δ is calculated and displayed along with the number of saturated sources, as well as the total simulation time. In order to obtain fast convergence, it has been noted that it is beneficial to keep the number of inner loop iterations relatively low, compared to the number of outer loop iterations, when dealing with a large amount of current sources. A great number of inner loop iterations would result in local convergence for one of the sources, but at the same time have greater impact on the surrounding sources. An incremental change in each source, however, will subsequently push all sources to convergence simultaneously.

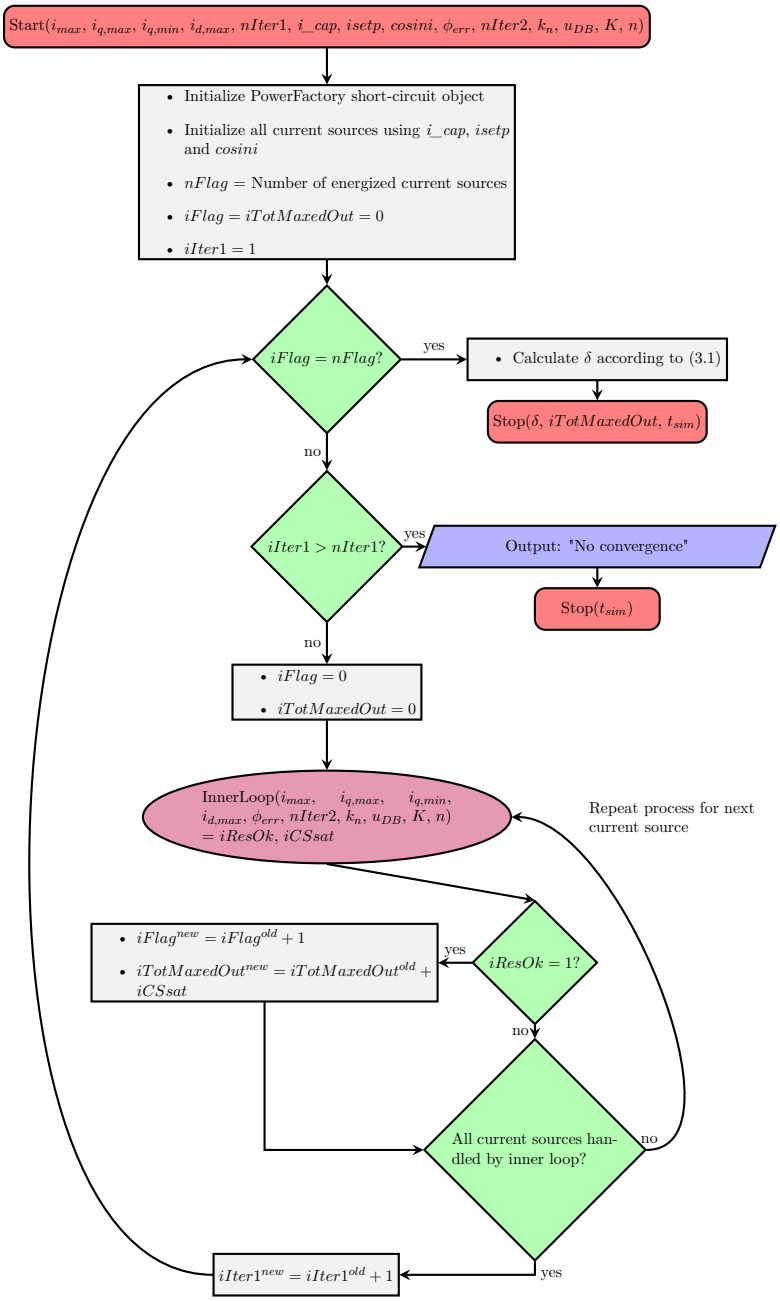

Figure 3.12. *Outer loop*

3.4 Wind Power Plant Aggregation Model

Consider the current source method described in the previous section. When dealing with a system model consisting of a large number of current sources, the convergence time of each simulation will be relevant. By aggregating the WTG arrays in the system, a considerably lower number of current sources could be used in model. By reducing the number of current sources handled by the iterative algorithm, the convergence time can be improved, which is important if a great number of studies are to be performed. For any fault occurring inside an array, a non-aggregated representation is still the only valid approach. This, however, does not prevent any remote WTG array in the system to be aggregated. A method used for WTG plant aggregation was originally proposed in [26]. Note that this method was initially intended for load-flow calculations. The remainder of this section will summarize selected parts of the method found the aforementioned article.

In figure 3.13 the generic representation of a WTG array can be found. Each WTG i is connected through a transformer T_i to a segment of the array cable. Let Z_i be the cable impedance separating WTG i from the subsequent WTG. Z_n represents the last stretch of cable connecting the array to the platform, with WTG n being the turbine closest to the platform. Assume that each turbine is operated at unity power factor, i.e. $\boldsymbol{S_i} = P_i$. Furthermore, each turbine is assumed to be operated at an equal voltage, that is $\boldsymbol{V_1} = \boldsymbol{V_2} = \cdots = \boldsymbol{V_n} = \boldsymbol{V}$. This assumption is never justified in the source material. In a real system the voltage, especially the voltage angle, will differ between each turbine in an array even during rated operation, since all generators are separated by complex impedances.

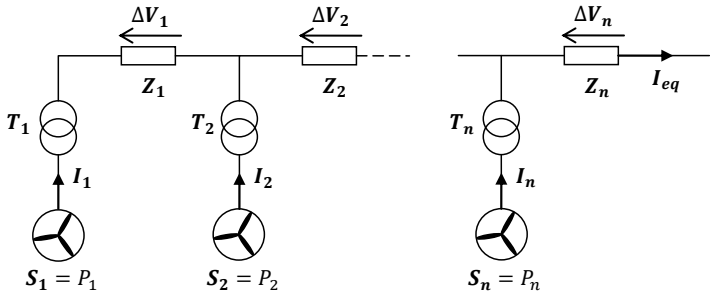

Figure 3.13. *Overview of a WTG array with n interconnected WTGs in series.*

For the following derivation, all values are assumed to be in per unit. Let the voltage drop across the cable impedance Z_1 be

$$\Delta \boldsymbol{V_1} = \boldsymbol{I_1 Z_1} = \frac{\boldsymbol{S_1}}{\boldsymbol{V}} \boldsymbol{Z_1} = \frac{P_1}{\boldsymbol{V}} \boldsymbol{Z_1}$$

where $\boldsymbol{I_i} = \boldsymbol{I_1}$ is the current of the first WTG. The voltage drop of the second

impedance $\boldsymbol{Z_2}$ will depend on the sum of the currents of WTG 1 and 2, i.e.

$$\Delta \boldsymbol{V_2} = (\boldsymbol{I_1} + \boldsymbol{I_2})\boldsymbol{Z_2} = (\frac{P_1}{\boldsymbol{V}} + \frac{P_2}{\boldsymbol{V}})\boldsymbol{Z_2}$$

From the above expression, it follows that the voltage drop across the n^{th} impedance will be

$$\Delta \boldsymbol{V_n} = (\boldsymbol{I_1} + \boldsymbol{I_2} + \cdots + \boldsymbol{I_n})\boldsymbol{Z_n} = (\frac{P_1}{\boldsymbol{V}} + \frac{P_2}{\boldsymbol{V}} + \cdots + \frac{P_n}{\boldsymbol{V}})\boldsymbol{Z_n}$$

The power loss in Z_1 can be written as

$$\boldsymbol{S_{Loss,Z_1}} = \Delta \boldsymbol{V_1}{\boldsymbol{I_1}}^* = \Big(\frac{P_1}{\boldsymbol{V}}\Big)\Big(\frac{{P_1}^*}{\boldsymbol{V}^*}\Big)\boldsymbol{Z_1} = \frac{{P_1}^2}{V^2}\boldsymbol{Z_1} = \frac{{P_{Z_1}}^2}{V^2}\boldsymbol{Z_1}$$

where $P_{Z_i} = P_{Z_1}$ is the active power transmitted through the impedance. From this it follows that

$$\boldsymbol{S_{Loss,Z_2}} = \Delta \boldsymbol{V_2}{\boldsymbol{I_2}}^* = \frac{(P_1 + P_2)^2}{V^2}\boldsymbol{Z_2} = \frac{{P_{Z_2}}^2}{V^2}\boldsymbol{Z_2}$$

and more generally

$$\boldsymbol{S_{Loss,Z_n}} = \Delta \boldsymbol{V_n}{\boldsymbol{I_n}}^* = \frac{(P_1 + P_2 + \cdots + P_n)^2}{V^2}\boldsymbol{Z_n} = \frac{{P_{Z_n}}^2}{V^2}\boldsymbol{Z_n}$$

The total loss in the array cable can be written as the sum of the above losses

$$\boldsymbol{S_{Loss}} = \frac{{P_{Z_1}}^2\boldsymbol{Z_1} + {P_{Z_2}}^2\boldsymbol{Z_2} + \cdots + {P_{Z_n}}^2\boldsymbol{Z_n}}{V^2} \tag{3.2}$$

Now consider the equivalent model found in figure 3.14. The WTGs found in figure 3.13 are now replaced by a generator producing a sum of the active power generated by each WTG in the non-aggregated model. The equivalent current $\boldsymbol{I_{eq}}$ flowing out of the WTG array should be equal in both the aggregated and non-aggregated model.

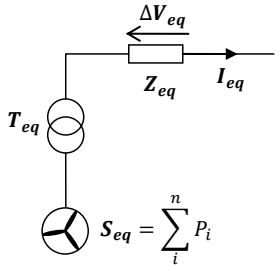

Figure 3.14. *Aggregated equivalent model of WTG array.*

The voltage drop across the equivalent array cable impedance Z_{eq} will thus be

$$\Delta \boldsymbol{V_{eq}} = \boldsymbol{I_{eq}}\boldsymbol{Z_{eq}} = \frac{(P_1 + P_2 + \cdots + P_n)}{\boldsymbol{V}}$$

since the total power transmitted through the equivalent impedance should be equal to that of the n^{th} impedance in the non-aggregated model. This is based on the assumption that the power loss in each cable segment is considerably smaller than the total transmitted power. The power loss in the equivalent impedance is expressed as

$$\boldsymbol{S_{Loss,Z_{eq}}} = \Delta \boldsymbol{V_{eq}} \boldsymbol{I_{eq}}^* = \boldsymbol{I_{eq}} \boldsymbol{I_{eq}}^* \boldsymbol{Z_{eq}} =$$

$$= \Big(\frac{P_1 + P_2 + \cdots + P_n}{\boldsymbol{V}}\Big)\Big(\frac{P_1 + P_2 + \cdots + P_n}{\boldsymbol{V}}\Big)^* \boldsymbol{Z_{eq}} =$$

$$= \frac{(P_1 + P_2 + \cdots + P_n)^2 \boldsymbol{Z_{eq}}}{V^2} = \frac{{P_{Z_n}}^2 \boldsymbol{Z_{eq}}}{V^2} \tag{3.3}$$

By setting (3.3) equal to (3.2) the following results are obtained

$$\frac{{P_{Z_n}}^2 \boldsymbol{Z_{eq}}}{V^2} = \frac{{P_{Z_1}}^2 \boldsymbol{Z_1} + {P_{Z_2}}^2 \boldsymbol{Z_2} + \cdots + {P_{Z_n}}^2 \boldsymbol{Z_n}}{V^2}$$

which can be rewritten as

$$\boldsymbol{Z_{eq}} = \frac{\sum_{i=1}^{n} {P_{Z_i}}^2 \boldsymbol{Z_i}}{{P_{Z_n}}^2} \tag{3.4}$$

In [26], the method for equivalencing the impedance of the aggregated WTG transformers, T_{eq}, is also described. For the purpose of this project, however, there is no need for this method. The transformer model used in PowerFactory allows for aggregation of two or more parallel transformers, which is the case for a WTG array in the above format. Similarly, the turbines can easily be aggregated, by using a current source with a rated current corresponding to the equivalent current I_{eq}.

When using this aggregation method, one should keep in mind that it is developed for load-flow simulations. The method can only be considered as valid for cases when all turbines are operated at a similar voltage. For certain operation scenarios, system configurations or high array cable impedances this may not always be the case.

Chapter 4

Numerical Results

In this chapter two case studies are performed and evaluated. From the results, general conclusions related to the current source method, are drawn.

4.1 Case Study: Single WTG connected to a Strong Grid

4.1.1 Introduction

The purpose of the case study is to illustrate the functionality of the current source method, while also demonstrating its performance. In addition to this, the static generator model in PowerFactory has been included in a test case for comparison. The case study is illustrating a single WTG connected through a transformer to a strong grid. The generating capacity of the WTG model is 100 MW, and simulates an aggregated OWPP where cable impedances have been neglected. Note that the purpose of the case study is not to illustrate a realistic short-circuit simulation, but rather provide a benchmark of the newly developed method.

4.1.2 Test System Overview

Consider the test system in figure 4.1(a). The FRC WTG is represented by both the current source model and the static generator. The WTG is connected to a external network model through a 2-winding transformer. The external network model represents a strong grid.

External network

The input parameters of the external network can be found in table 4.1. In order for the external network to act as a strong grid, the load-flow characteristics have been selected as a slack type with nominal voltage $1\angle 0^\circ$ p.u.. The choice of short-circuit power, and impedance ratio, are depending on the strength and characteristics of the modeled grid. With no available information of a real life grid model, these parameters need to be selected based on assumptions. In order to model a strong

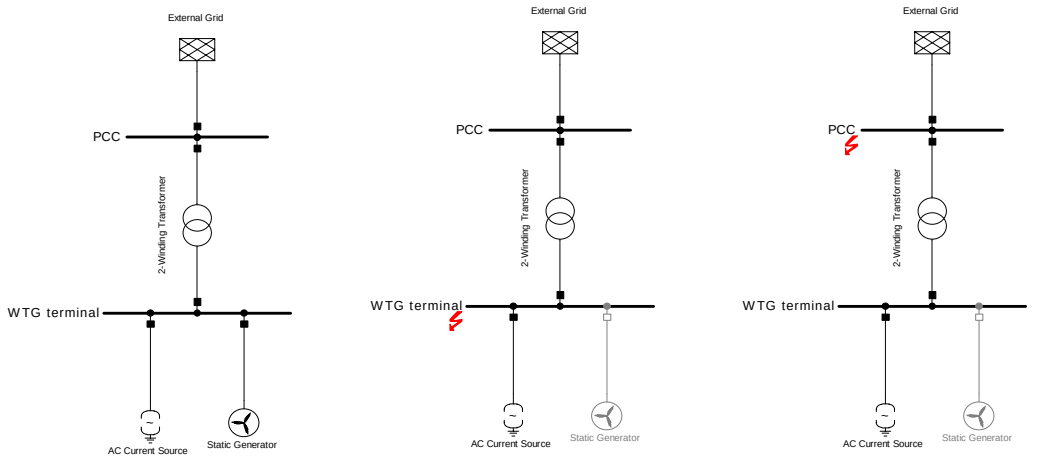

(a) *PowerFactory test system overview*

(b) *Overview fault case 1*

(c) *Overview fault case 2*

Figure 4.1. *Overview of the case study.*

grid, the Short-Circuit Ratio (SCR) needs to be considered [36]. The SCR is the ratio between generated power and assumed short-circuit power of the connected grid. The SCR of a strong grid is discussed through out the literature and considered to be anywhere from SCR > 2 [37] to SCR > 25 [38]. For this case study, the SCR has been selected as 10. In other words, the short-circuit power S''_k of the external network is 1000 MVA, since the generated power is 100 MW. The impedance ratio has been set to 0.1, in order to represent a mainly inductive grid. In accordance with the IEC 60909 standard, the voltage factor has been set to 1.1, since the voltage level of the bus connection is 33 kV. By using a voltage correction factor of 1.1 the level of conservativeness is increased.

Table 4.1. *Input parameters of the external network model.*

Parameter	Description	Value
u	Nominal voltage	1 p.u.
φ	Voltage angle	0°
S''_k	Short-circuit power	1000 MVA
r_1	Impedance ratio	0.1
c_{max}	Voltage factor	1.1

2-winding transformer

The input parameters of the 2-winding transformer can be found in table 4.2. For this case study, the transformer winding setup is *YNyn0*, a Y-connection with

grounded neutral at both the high and low voltage side. The transformer is operating at a fixed turns ratio without an OLTC. The selection of impedance is arbitrary, but in the range of what could be expected for a high power transformer.

Table 4.2. *Input parameters of the 2-winding transformer model.*

Parameter	Description	Value
S_n	Rated power	100 MVA
U_h/U_l	Voltage ratio	33/0.69 kV
x_1	Positive sequence reactance	0.01 p.u.
R/X''	Positive sequence resistance	0.001 p.u.

Static generator

The input parameters of the static generator can be found in table 4.3. The choice of short-circuit power is such that the resulting subtransient short-circuit is equal to the rated current.

Table 4.3. *Input parameters of the static generator model.*

Parameter	Description	Value
S_n	Rated power	100 MVA
$\cos\phi$	Power factor	1.0
P	Generated active power	100 MW
S_k''	Short-circuit power	100 MVA
R/X''	Short-circuit impedance ratio	0.1

Current source

The rated current of the current source is set to 83.674 kA, i.e.

$$I_n = \frac{P_n}{\sqrt{3} \cdot U_n^{690\text{V}}} = \frac{100 \text{ MW}}{\sqrt{3} \cdot 690 \text{ V}} = 83.674 \text{ kA}$$

4.1.3 Test Cases

In order to illustrate the capabilities of the current source method, four test cases have been developed, in order to illustrate the effect of using different method input parameters. These can be found in table 4.4. The input parameters were arbitrarily chosen, in order to illustrate the flexibility of the developed method.
Furthermore, in each test case the system has been subject to the following faults:

Table 4.4. *Current source method input parameters for test case 1-4.*

Test case	i_{max}	$i_{q,max}$	$i_{d,max}$	$i_{q,min}$	K	u_{DB}	n
1	1.0	1.0	1.0	0	2.0	0.1	100
2	1.4	1.0	1.4	0	2.0	0.1	100
3	1.0	1.0	1.0	0	2.5	0.05	100
4	1.1	1.1	1.0	0.4	2.0	0.1	25

- *Fault 1*: Three-phase line-to-ground fault at the WTG terminal, see figure 4.1(b).
- *Fault 2*: Three-phase line-to-ground fault at the PCC, i.e. the connection of the external network, see figure 4.1(c).

In both above cases, the fault impedance $|\boldsymbol{Z_f}| = |R_f + jX_f| = Z_f$ has been varied such that the voltage drop obtained at the WTG terminal is $0 < \Delta u < 1$. The fault impedance ratio has been kept at fixed ratio $X_f/R_f = 5$. This is a seemingly arbitrary choice, but selected in order to obtain a mainly inductive resulting short-circuit impedance, as seen from the WTG generator. In addition to this, it allows for comparison with previous studies [21, 39].

For the sake of comparison, the static generator has been included in test case 1 for both fault case 1 and 2. Note, however, that the only comparable results for the current source method and static generator is the total short-circuit current for a given fault impedance $|Z_f|$. This is a testament to the fact that no more information is available to the user, as was described in Section 1.4. To make any claims about the active and reactive power flow of the steady-state behavior of the static generator, the corresponding voltage angle of the terminal needs to be known. The current angle can, however, give some hints of the behavior of the generator.

4.1.4 Comments on the Results

The purpose of this section is to provide some brief comments on the obtained case study results. For more in depth conclusions drawn from the results, see Section 4.3.

In each test case, when utilizing the current source method, the reactive and active current component, deviation factor δ and simulation time is plotted as a function of the WTG terminal voltage drop Δu. The simulated current components are plotted against the corresponding reference curve. See figure 4.2 and 4.5 - 4.7.

Test case 1 comparison

In figure 4.2, the simulation results obtained for the current source method are available. As it can be seen in figure 4.2(a) and 4.2(b), the method successfully

obtains the reference values set by the grid code, in both fault cases. In figure 4.2(c) and 4.2(d), the corresponding deviation factor δ simulation time are plotted, respectively.

In figure 4.3 and 4.4, the simulation results of the current source method and static generator are compared for fault case 1 and 2. In figure 4.3(a) and 4.4(a), the total short-circuit current is plotted as a function of the fault impedance. The current source provides a constant output current for the whole range, as expected. The static generator current generator experiences a sag for the fault impedance range corresponding to linear reactive current ramping of the current source. This can be seen in figure 4.3(b) and 4.4(b). Note, that the active and reactive current component denoted with the superscript †, are not the true values, but based on the current angle solely. Given the striking similarities between the current components found in 4.3(b), 4.3(c), 4.4(b) and 4.4(c), the voltage angle of the static generator terminal can be assumed to be neglectable for the full range of fault impedances. Other than the deviation in the total current, the lack of a discontinuity in $i^{\dagger}_{q,StatGen}$ is noteworthy. If $i^{\dagger}_{q,StatGen}$ in fact is close to the true value of the reactive current, then it appears as if $i_{q,StatGen}$ is ramped down linearly to 0. These results can be interpreted as consistent with the grid code voltage control curve, which the current iteration method is based upon [24]. If this indeed is the intended behavior of the static generator, it indicates that the current iteration method is not applicable for the case when the FRC WTGs are used in a study based on the E.ON voltage control curve, found in figure 2.5.

Current source method, test case 1 - 4

Overall, it can be concluded that the obtained results correspond to the reference values. There are, however, some notable deviations. As it can be seen in figure 4.2(b), 4.5(a), 4.5(b), 4.6(b) and 4.7(b), the method does not converge to the correct reference value for voltage drops close to 1 p.u.. In all test cases, this is reflected by a deviation factor close to 1 %. Note that this only occurs for the second fault case, i.e. at the PCC.

Consider δ in figure 4.2(c) and 4.5(c) - 4.7(c). In all test cases, there is a peak in δ above 10 % for $\Delta u < u_{DB}$. The cause for this is the difference between simulated value and the expected "real" reference value. The calculation of δ is based on a reference curve without a smoothing function. This will result in an increasing difference between the "real" reference value and the one obtained using the smoothing function, as Δu is increased closer to u_{DB}.

Also, the simulation time for the same voltage range mentioned is considerably higher, see figure 4.2(d) and 4.5(d) - 4.7(d). This is due to the fact that for voltage drops close to u_{DB}, the active current is at its maximum, and for this system setup this corresponds to a current source power factor close to 1. In the method

implementation, the incremental change of the power factor is kept small for $\cos\phi$ close to 1 to avoid overshoot.

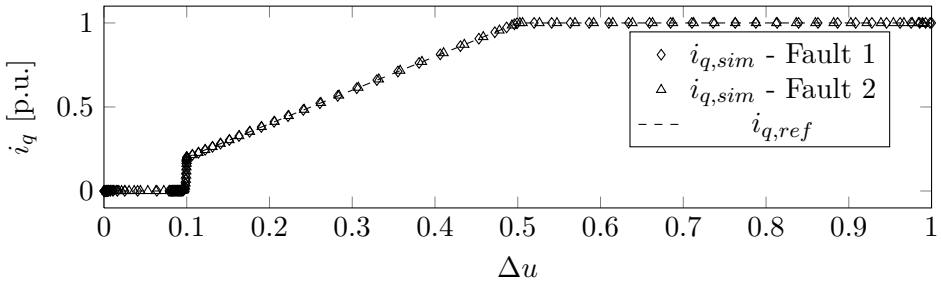

(a) *Reactive current component* i_q

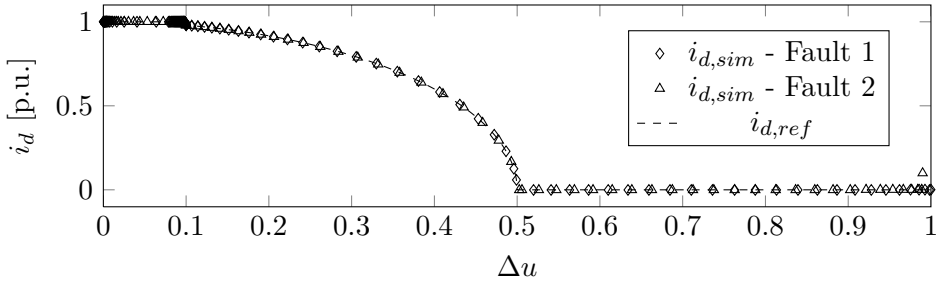

(b) *Active current component* i_d

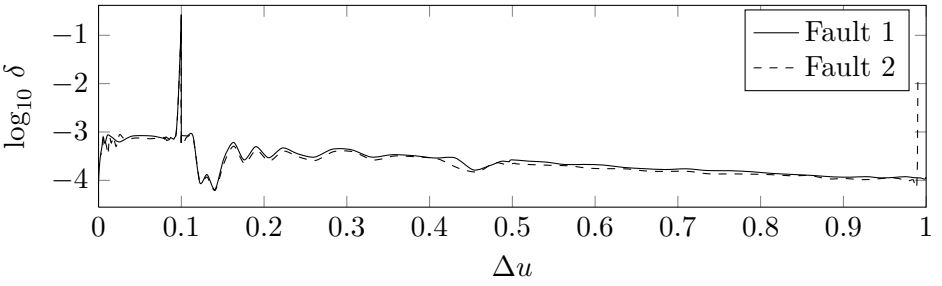

(c) *Deviation factor* δ

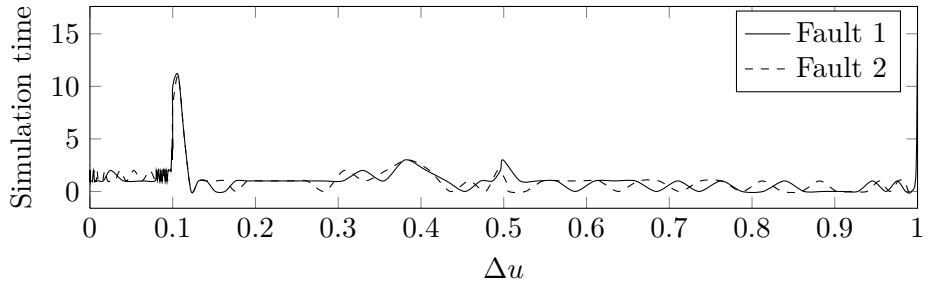

(d) *Simulation time*

Figure 4.2. *Current source method simulation results for test case 1.*

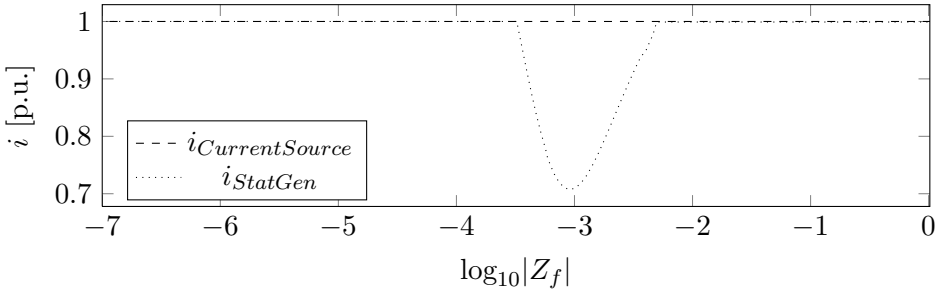

(a) *Total short-circuit current*

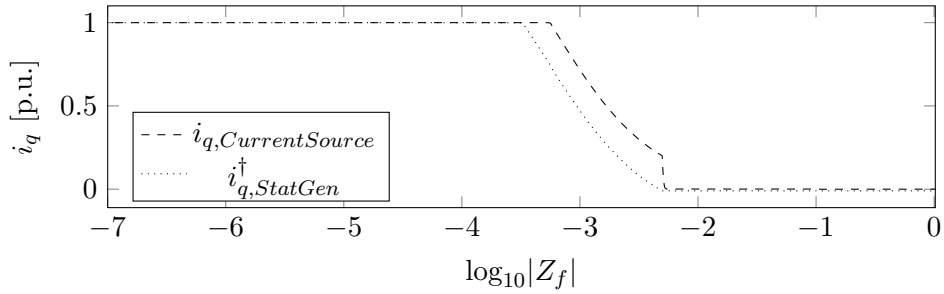

(b) *Reactive current component*

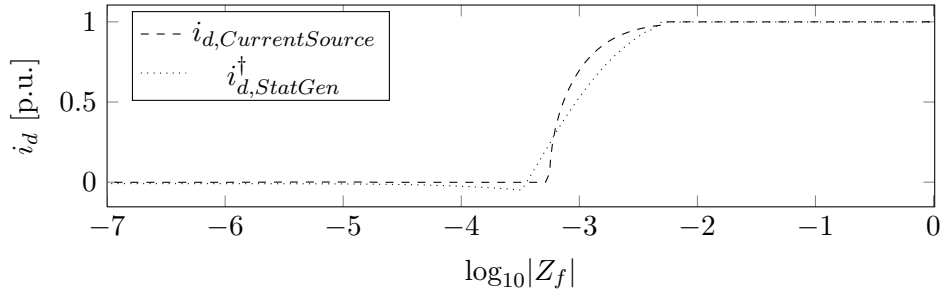

(c) *Active current component*

Figure 4.3. *Simulation results for test case 1 - fault 1: Comparison between results obtained using the current source method and the static generator model with current iteration.*

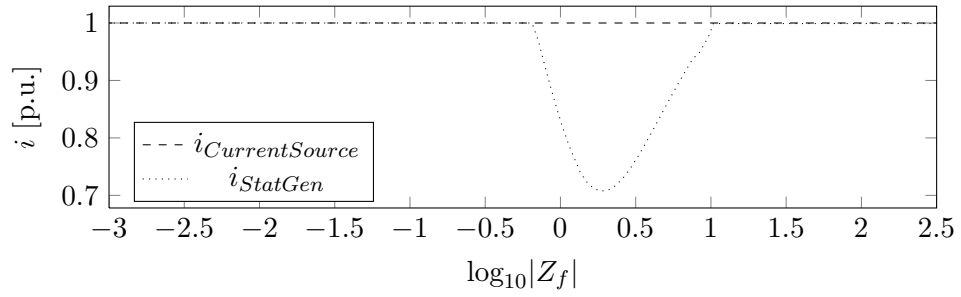

(a) *Total short-circuit current*

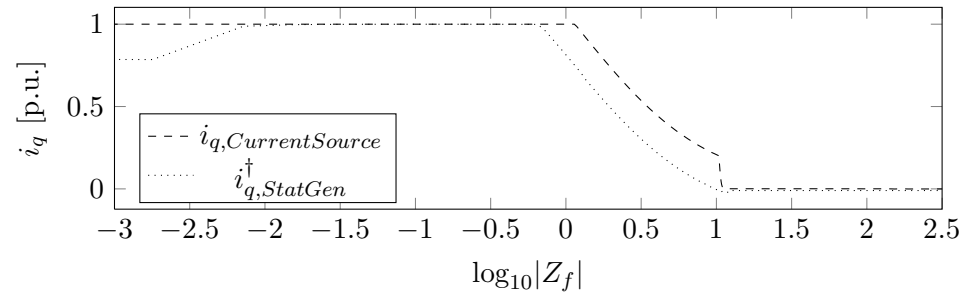

(b) *Reactive current component* i_q

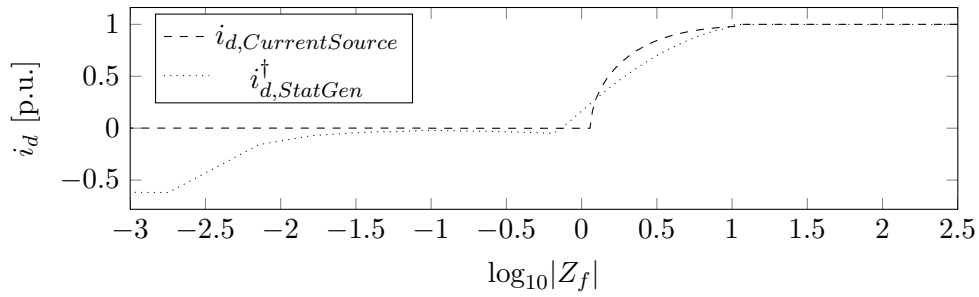

(c) *Active current component* i_d

Figure 4.4. *Simulation results for test case 1 - fault 2: Comparison between results obtained using the current source method and the static generator model with current iteration.*

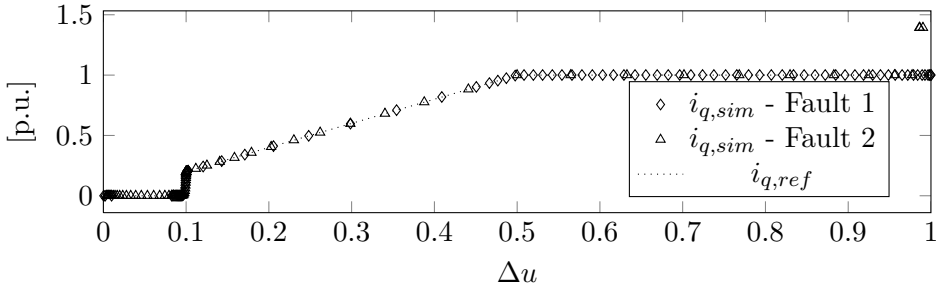

(a) *Reactive current component* i_q

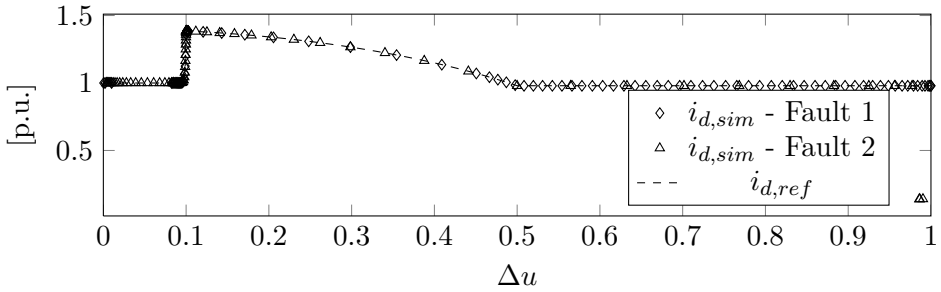

(b) *Active current component* i_d

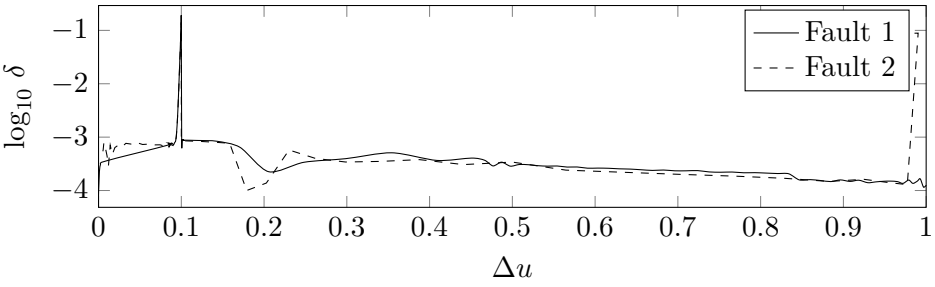

(c) *Deviation factor* δ

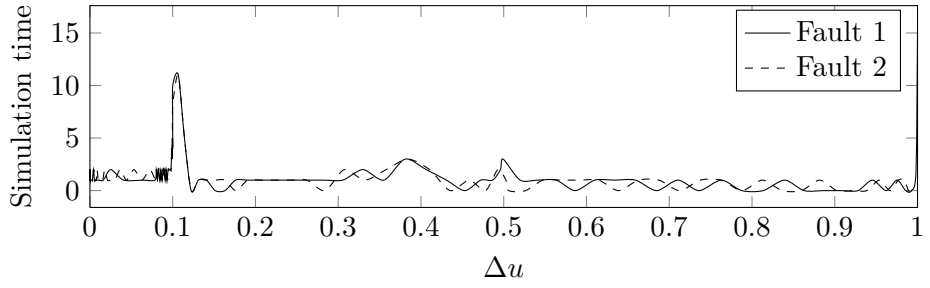

(d) *Simulation time*

Figure 4.5. *Current source method simulation results for test case 2.*

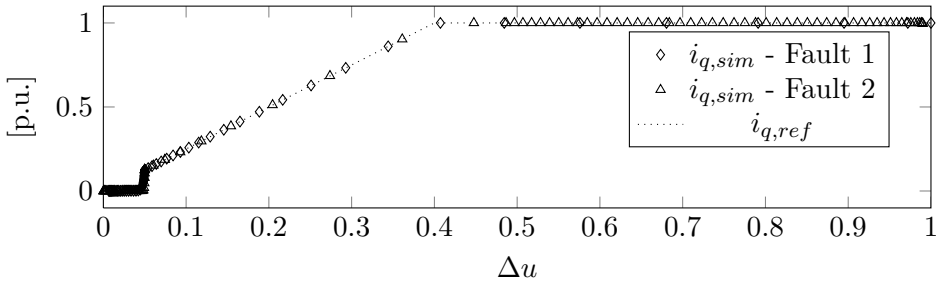

(a) *Reactive current component* i_q

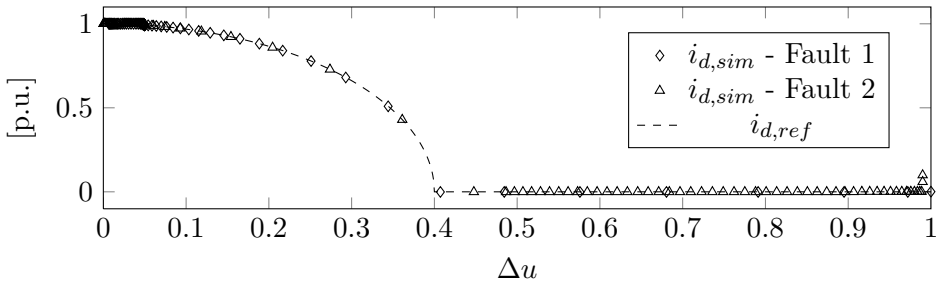

(b) *Active current component* i_d

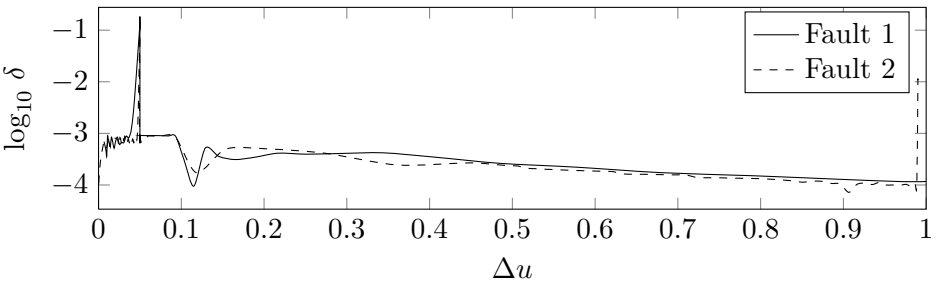

(c) *Deviation factor* δ

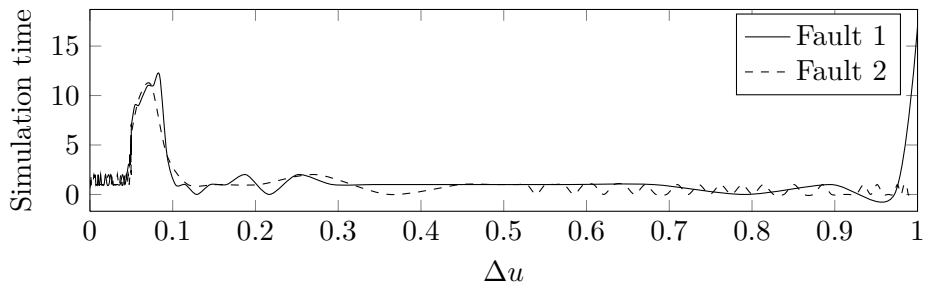

(d) *Simulation time*

Figure 4.6. *Current source method simulation results for test case 3.*

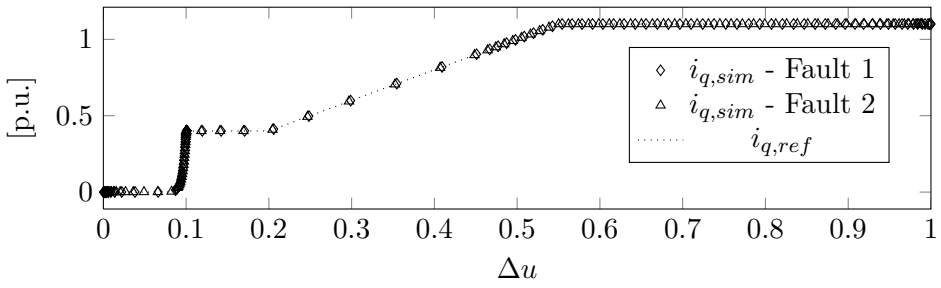

(a) *Reactive current component i_q*

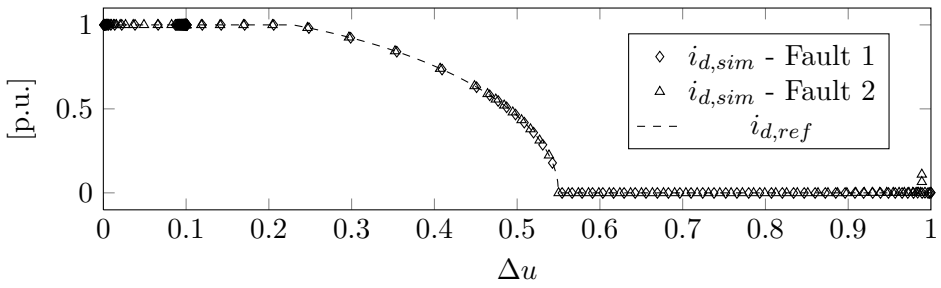

(b) *Active current component i_d*

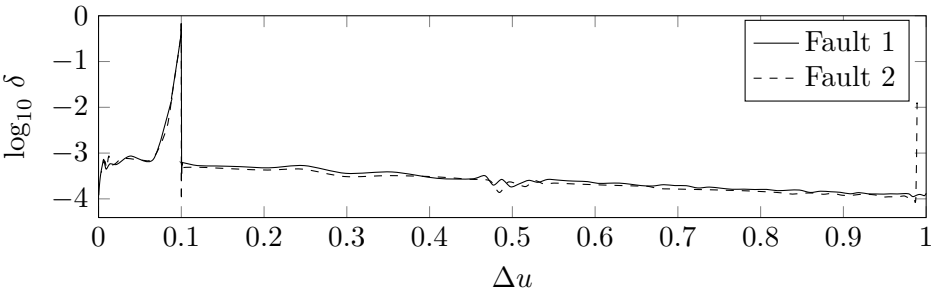

(c) *Deviation factor δ*

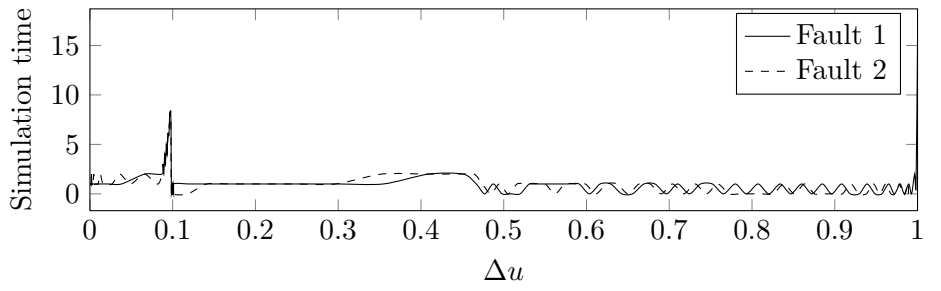

(d) *Simulation time*

Figure 4.7. *Current source method simulation results for test case 4.*

4.2 Case Study: Offshore Wind Power Plant

4.2.1 Background Description

The purpose of the case study is to illustrate the current source method in a larger test system. The test system will be subject to several short-circuits, and the effectiveness of the current source method, and model aggregation is evaluated. In order to illustrate a realistic short-circuit study, a test system based on a plausible system investigated by ABB. The component parameters used within the system are based on proposed components, but have been slightly altered due to corporate secrecy. All results are obtained using the system model in PowerFactory and post-calculated values are based on simulation data.

4.2.2 Test System Overview

In figure 4.8, an overview of the test system model in PowerFactory, can be found. An external network model is connected at the PCC, in order to model a strong grid connection. The onshore substation connected to the PCC utilizes two onshore transformers. The onshore substation is connected to two offshore platforms by a land and a subsea cable. Each offshore platform utilizes two power transformers, which subsequently are connected to one of four WTG collection grids. Each collection grid is here modeled by a single array consisting of ten WTGs, with an individual rated power of 5 MW. Note that the collection grid of an OWPP usually consists of several WTG arrays. For this case study, the number of arrays per collection grid has been reduced, to provide a simpler model. With ten turbines in each array, and four arrays in total, the OWPP therefore produces a total of 200 MW.

The system is designed in a symmetrical fashion, i.e. the left and right branch as seen from the onshore substation are identical. This, of course, is not completely realistic, but assumed for the purpose of this case study. The WTG array is modeled separate from the main system. In figure 4.9, the array connection is depicted. This includes both an aggregated model of the array and a non-aggregated plant, modeled separately. For any type of fault applied upstream of the array connection, i.e. anywhere in the system from the WTG array connection to the PCC, the aggregated model is used. All faults applied within the array is based on the non-aggregated model. As an example, consider a fault applied within one of the arrays. This part of the system will use the non-aggregated model while the three remaining arrays, which are remote to the fault location, are aggregated.

The aggregated model consists of an aggregated array cable, transformer and WTG model. The non-aggregated array can be found in figure 4.10. The first WTG in the array is connected directly to the array cable found in figure 4.9, while each subsequent model is connected in parallel through an additional segment of array cable.

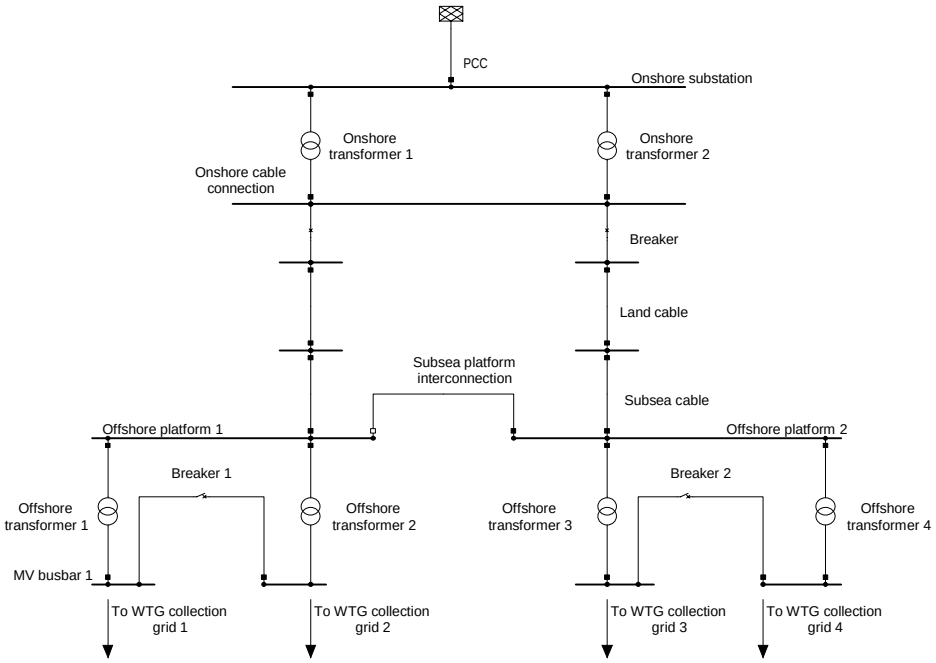

Figure 4.8. *PowerFactory model of OWPP.*

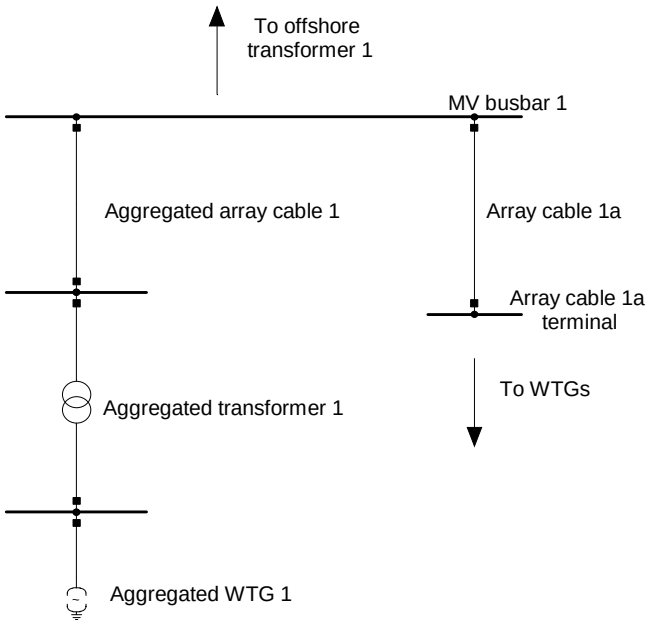

Figure 4.9. *PowerFactory model of OWPP WTG array connection.*

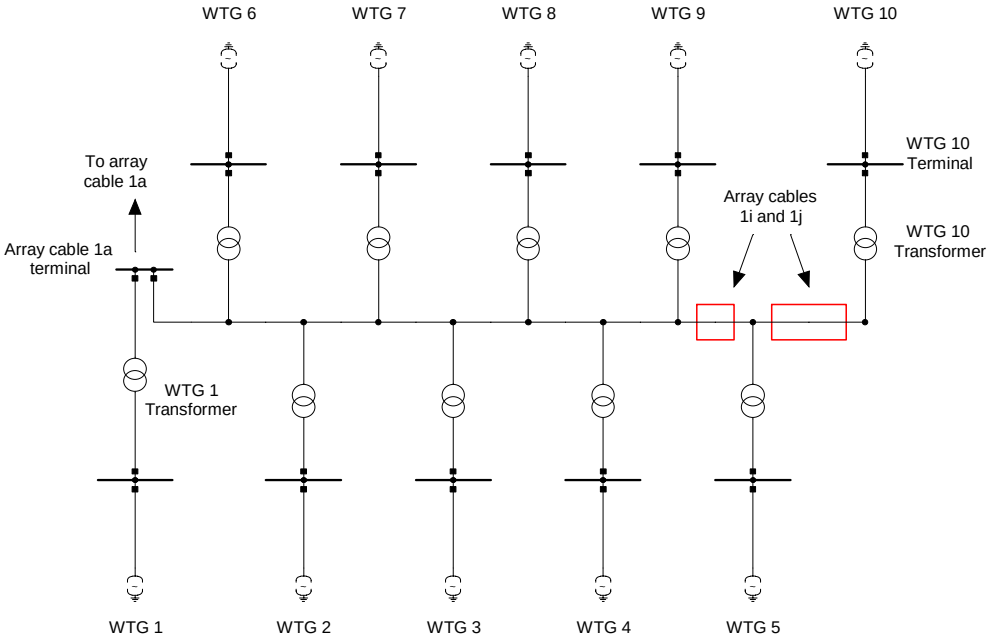

Figure 4.10. *PowerFactory model of OWPP WTG array.*

Each array is placed at a distance of 2.5 km from the offshore platform, and the length of each array cable interconnecting the turbines is 700 m. Furthermore, each WTG is connected to the array cable through a WTG transformer. In table 4.5 and 4.6, the parameter values used for the system transformers and cables, respectively, can be found. The impedance of the aggregated array cables are calculated using (3.4) found in Section 3.4. With each turbine producing $P = 5$ MW, the aggregated impedance of the array cables is calculated as follows

$$\boldsymbol{Z_{eq}} = \frac{\sum_{i=1}^{n} {P_{Z_i}}^2 \boldsymbol{Z_i}}{{P_{Z_n}}^2} = \frac{\sum_{i=1}^{9} (i \cdot P)^2 \boldsymbol{Z'} + (10 \cdot P)^2 \boldsymbol{Z''}}{(10 \cdot P)^2} =$$

$$= 0.3495 + j0.4495 \ \Omega/\text{km}$$

where $\boldsymbol{Z'}$ is the impedance of each segment of the array cable, and $\boldsymbol{Z''}$ is the impedance of the array cable connecting the first WTG in the array to the platform. The parallel transformers in each array can be aggregated in PowerFactory using the same transformer data as the non-aggregated model. The transformer model used for the aggregated model simply needs to be set as 10 parallel transformers in the basic options. Each WTG is modeled using an AC current source with a rated current of 4183.69 A (non-aggregated) or 41836.9 A (aggregated). This is calculated from

$$I_{n,non-agg} = \frac{P_n}{\sqrt{3} \cdot U_{n,WTG}} = \frac{5 \text{ MW}}{\sqrt{3} \cdot 690 \text{ V}} = 4183.69 \text{ A}$$

$$I_{n,agg} = \frac{10 \cdot P_n}{\sqrt{3} \cdot U_{n,WTG}} = \frac{50 \text{ MW}}{\sqrt{3} \cdot 690 \text{ V}} = 41836.9 \text{ A}$$

The external network is modeled as a slack bus with a fixed voltage of $1\angle 0°$ p.u.. The short-circuit behavior of the external network is modeled using the following parameters:

- $S''_k = 5000$ MVA - Based on a total generated power of 200 MW (SCR = 25).
- $R/X = 0.1$ - Representing a mainly inductive grid.
- $c_{max} = 1.1$ - Introducing a level of conservativeness.

Note that the SCR = 25 in order to represent a very strong grid.

Table 4.5. *Transformer model parameters.*

Transformer	Voltage rating	Rated power	x_1	r_1	Type
Onshore	400/220 kV	200 MVA	0.12 p.u.	0.002 p.u.	YNyn0
Offshore	220/33 kV	50 MVA	0.12 p.u.	0.003 p.u.	YNyn0
WTG	33/0.69 kV	5 MVA	0.08 p.u.	0.006 p.u.	Dyn11

Table 4.6. *Cable model parameters.*

Cable	Voltage rating	Length	X/km	R/km
Land cable	220 kV	30 km	0.18 Ω	0.075 Ω
Subsea cable	220 kV	40 km	0.1 Ω	0.065 Ω
Subsea platform interconnection	220 kV	10 km	0.1 Ω	0.065 Ω
Array cable	33 kV	2.5 km	0.1 Ω	0.06 Ω
WTG interconnection cable	33 kV	0.7 km	0.1 Ω	0.1 Ω
Aggregated array cables	33 kV	1 km	0.4495 Ω	0.3495 Ω

4.2.3 Test Cases

In order to illustrate the behavior of the current source method, and to illustrate the short-circuit contribution from multiple FRC WTGs, several test cases have been developed for the case study.

First, a load-flow simulation and short-circuit calculation is performed, in order to verify the accuracy of the aggregated impedance model used for the aggregated WTG array. For the load-flow simulation, all current sources, both aggregated and non-aggregated, are set according to the following parameters:

- $i_{setp} = -1$

- $i_{cap} = 0$
- $cos\phi = 1$

Using these settings, each source will generate a load-flow current corresponding to the rated active power of each WTG. The short-circuit calculation is performed for a bolted fault applied directly to the WTG array connection seen in figure 4.9. Both of the above cases are considered for a system operating according to a normal operation scenario (scenario 1) which is explained below.

Secondly, fault cases in which a bolted fault is applied at one of the following busbars are considered:

- Fault case 1: PCC - 400 kV busbar interconnecting the OWPP to the external network, see figure 4.8.
- Fault case 2: Onshore cable connection - Low voltage side of onshore substation (220 kV), see figure 4.8.
- Fault case 3: Offshore platform 1 - High voltage side of offshore platform 1 (220 kV), see figure 4.8.
- Fault case 4: MV busbar 1 - Medium voltage side of offshore platform 1 (33 kV), see figure 4.8 or 4.9.
- Fault case 5: Array cable 1a terminal - Connection point at the end array cable 1a (33 kV), see figure 4.10.
- Fault case 6: WTG Terminal 10 - Terminal of WTG 10 (0.69 kV), see figure 4.10.

Furthermore, for each test case the system is operated according to the two following scenarios

- Scenario 1: Normal operation - Onshore transformer 1 and 2 are both connected to reduce transmission losses. The subsea platform interconnection is disconnected and both breaker 1 and 2 are open. In other words, each transformer in the system is operated at half the rated power, i.e. the offshore transformer at 100 MW and onshore transformer at 200 MW. This scenario is depicted in figure 4.8.
- Scenario 2: Contingency operation - This scenario illustrates the case when the short-circuit impedance of the system is at its lowest. Both onshore transformers are still connected. The subsea platform interconnection is connected reducing the effective impedance between the offshore platforms and the land connection by half. Also, both breaker 1 and 2 are closed thus reducing the effective offshore transformer impedance by half.

For the calculation of $i_{d.c.}$ and I_{th} the break time $t = 0.1$ s and fault clearing time $T_k = 1$ s were used.

4.2.4 Results

All short-circuit simulation results were obtained using the algorithm input parameters listed in table 4.7. In each fault case, the fault location was selected accordingly, and the fault impedance $\boldsymbol{Z_f}$ was kept at 0 Ω. All current components, other than the transient/steady-state short-circuit current, was calculated using *Method C(1)*.

Table 4.7. *Algorithm input parameters used in case study 2.*

i_{max}	$i_{q,max}$	$i_{q,min}$	$i_{d,max}$	$nIter1$	i_{cap}	i_{setp}
1.0	1.0	0.0	1.0	100	1	1
$\cos\phi$	ϕ_{err}	$nIter2$	k_n	u_{DB}	K	n
0.1	0.05	10	1.0	0.1	2.0	100

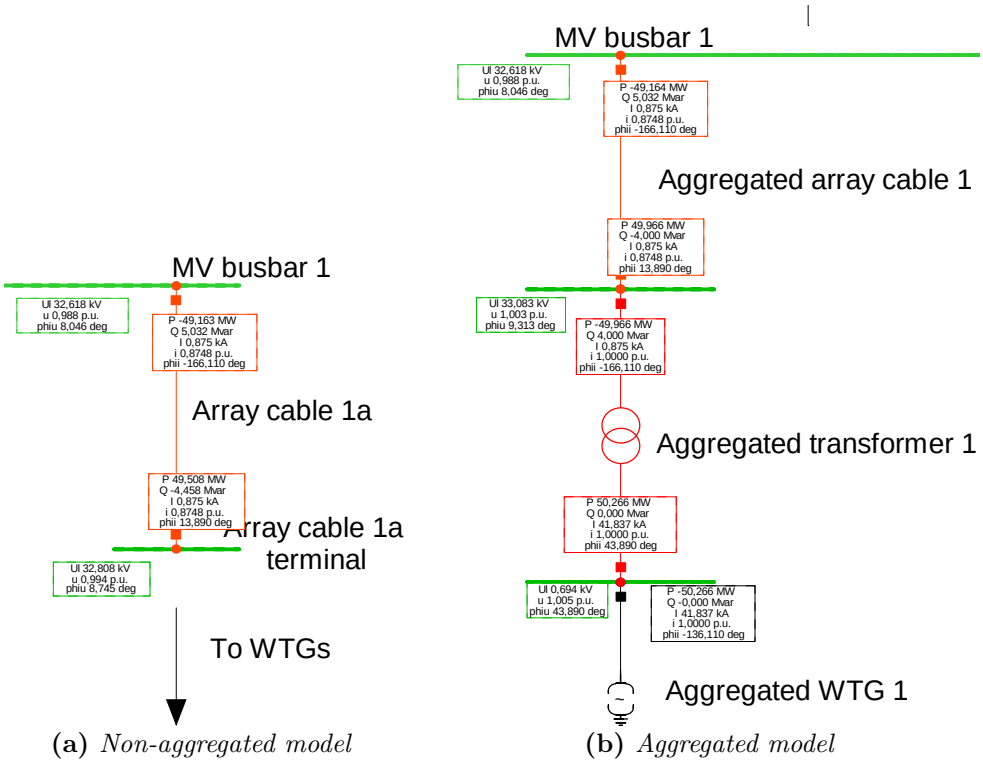

(a) *Non-aggregated model* **(b)** *Aggregated model*

Figure 4.11. *Load-flow results for the non-aggregated and aggregated array model.*

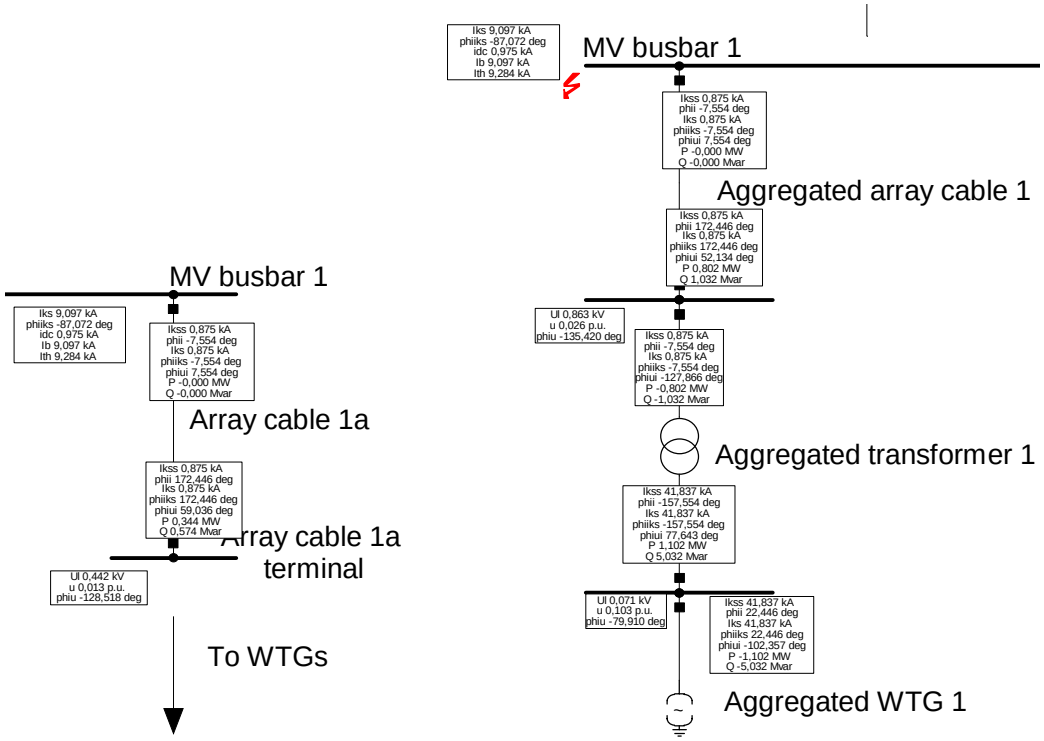

(a) *Non-aggregated model* **(b)** *Aggregated model*

Figure 4.12. *Short-circuit calculation results for the aggregated and non-aggregated array model.*

Impedance aggregation model

In figure 4.11(a) and 4.11(b), the load-flow results obtained for the non-aggregated and aggregated array can be found. For both cases, the same bus voltage and equivalent current in the array cable are obtained. Note that the relevant result box used for comparison of transmitted power and current is the red box positioned closest to the green busbar at the top. The power flow P and Q are here defined as flowing into the array cable, and it can be seen in both cases, that the delivered power at this node is 49.974 MW at a voltage of 1.005 p.u. and current of 0.8748 p.u..

Similar to the above case, the short-circuit results used for comparing the non-aggregated and aggregated array models can be found in figure 4.12(a) and 4.12(b), respectively. Here, the resulting transient short-circuit current in the busbar, as well as $i_{d.c.}$, I_b and I_{th} are equal in both cases. As it can be seen in the figure, the resulting short-circuit current produced by the non-aggregated and aggregated WTG array are equal.

Fault cases

In table 4.8-4.13, the results obtained for each WTG in fault case 1 - 6 are listed. In each scenario, the resulting terminal voltage u is reported, along with the corresponding reactive current reference value $i_{q,ref}$, the simulated reactive current $i_{q,sim}$ and the absolute error between the two, $i_{q,err} = |i_{q,sim} - i_{q,ref}|$. In table 4.14 and 4.15 the results obtained for each busbar in scenario 1 and 2 are displayed. Here, the transient short-circuit current I'_k corresponding to the steady-state current is displayed. In addition to this, the following results are provided:

- Conservative estimate of the total short-circuit current $I'_{k,\delta}$. This value is post-calculated based on the obtained value of I'_k and δ.
- Decaying DC component $i_{d.c.}$.
- Symmetrical breaking current I_b.
- Thermal equivalent current I_{th}.
- Deviation factor δ.
- Simulation time t.

The results for fault case 6 were obtained using $k_n = 0.9$. The nudge factor was applied to decrease the incremental change in between iterations, since a problem with convergence was detected.

As can be seen in table 4.8 and 4.9, there is no difference in the obtained results for scenario 1 and 2 for fault case 1 and 2. This is because the OWPP is separated into two symmetrical systems, i.e. the contingency in scenario 2 does not affect the resulting voltage drop on each WTG terminal. The maximum error obtained when using only aggregated source models is obtained for fault case 4, scenario 2. This can be seen in table 4.11. Here, the error for the aggregated arrays located closest to the fault location is 2.3 %. This is reflected by $\delta = 2.7$ %, found in table 4.15. Note that this is the most severe deviation obtained from all of the simulation results. With a deviation factor of 2.7 %, the conservative estimate $I'_{k,\delta}$ is therefore 5.4 % larger than the simulated total short-circuit current.

In table 4.13, another noteworthy result can be found. For scenario 1, numerous current sources are operated at a voltage drop very close to the dead band voltage. Because of the smoothing function introduced in Section 3.3.2, a large error is increased where the largest amounts to 17.9 %. When studying the results in table 4.14, for the same fault case, one can note that even though the fault is quite severe for a number of sources, the overall deviation factor δ is 1.8 %. This deviation is in other words lower than what was obtained in the worst case results for fault case 4, scenario 2.

Table 4.8. *Simulation results for a bolted fault at the PCC (fault case 1), during normal operation (scenario 1) and contingency operation (scenario 2). All values are in p.u..*

	Scenario 1				Scenario 2			
Source	u	$i_{q,ref}$	$i_{q,sim}$	$i_{q,err}$	u	$i_{q,ref}$	$i_{q,sim}$	$i_{q,err}$
Agg. WTG 1	0.243	1.000	0.990	0.010	0.243	1.000	0.990	0.010
Agg. WTG 2	0.243	1.000	0.990	0.010	0.243	1.000	0.990	0.010
Agg. WTG 3	0.243	1.000	0.990	0.010	0.243	1.000	0.990	0.010
Agg. WTG 4	0.243	1.000	0.990	0.010	0.243	1.000	0.990	0.010

Table 4.9. *Simulation results for a bolted fault at the onshore cable terminal (fault case 2), during normal operation (scenario 1) and contingency operation (scenario 2). All values are in p.u..*

	Scenario 1				Scenario 2			
Source	u	$i_{q,ref}$	$i_{q,sim}$	$i_{q,err}$	u	$i_{q,ref}$	$i_{q,sim}$	$i_{q,err}$
Agg. WTG 1	0.183	1.000	0.983	0.017	0.183	1.000	0.983	0.017
Agg. WTG 2	0.183	1.000	0.983	0.017	0.183	1.000	0.983	0.017
Agg. WTG 3	0.183	1.000	0.983	0.017	0.183	1.000	0.983	0.017
Agg. WTG 4	0.183	1.000	0.983	0.017	0.183	1.000	0.983	0.017

Table 4.10. *Simulation results for a bolted fault at the offshore platform 1 busbar (fault case 3), during normal operation (scenario 1) and contingency operation (scenario 2). All values are in p.u..*

	Scenario 1				Scenario 2			
Source	u	$i_{q,ref}$	$i_{q,sim}$	$i_{q,err}$	u	$i_{q,ref}$	$i_{q,sim}$	$i_{q,err}$
Agg. WTG 1	0.162	1.000	0.989	0.011	0.162	1.000	0.989	0.011
Agg. WTG 2	0.162	1.000	0.989	0.011	0.162	1.000	0.989	0.011
Agg. WTG 3	0.490	1.000	1.000	0.000	0.166	1.000	0.999	0.001
Agg. WTG 4	0.490	1.000	1.000	0.000	0.166	1.000	0.999	0.001

Table 4.11. *Simulation results for a bolted fault at the MV busbar 1 (fault case 4), during normal operation (scenario 1) and contingency operation (scenario 2). All values are in p.u..*

	Scenario 1				Scenario 2			
Source	u	$i_{q,ref}$	$i_{q,sim}$	$i_{q,err}$	u	$i_{q,ref}$	$i_{q,sim}$	$i_{q,err}$
Agg. WTG 1	0.103	1.000	0.977	0.023	0.103	1.000	0.977	0.023
Agg. WTG 2	0.732	0.536	0.537	0.001	0.103	1.000	0.977	0.023
Agg. WTG 3	0.817	0.366	0.366	0.000	0.639	0.723	0.722	0.000
Agg. WTG 4	0.817	0.366	0.366	0.000	0.639	0.723	0.723	0.000

Table 4.12. *Simulation results for a bolted fault at the array cable 1a terminal (fault case 5), during normal operation (scenario 1) and contingency operation (scenario 2). All values are in p.u..*

	Scenario 1				Scenario 2			
Source	u	$i_{q,ref}$	$i_{q,sim}$	$i_{q,err}$	u	$i_{q,ref}$	$i_{q,sim}$	$i_{q,err}$
WTG 1	0.080	1.000	0.997	0.003	0.080	1.000	0.997	0.003
WTG 2	0.086	1.000	0.991	0.009	0.086	1.000	0.991	0.009
WTG 3	0.091	1.000	0.985	0.015	0.091	1.000	0.985	0.015
WTG 4	0.094	1.000	0.981	0.019	0.094	1.000	0.981	0.019
WTG 5	0.096	1.000	0.978	0.022	0.096	1.000	0.978	0.022
WTG 6	0.083	1.000	0.994	0.006	0.083	1.000	0.994	0.006
WTG 7	0.089	1.000	0.988	0.012	0.089	1.000	0.988	0.012
WTG 8	0.093	1.000	0.983	0.017	0.093	1.000	0.983	0.017
WTG 9	0.096	1.000	0.979	0.021	0.096	1.000	0.979	0.021
WTG 10	0.097	1.000	0.977	0.023	0.097	1.000	0.977	0.023
Agg. WTG 2	0.762	0.476	0.476	0.000	0.294	1.000	1.000	0.000
Agg. WTG 3	0.840	0.320	0.320	0.000	0.699	0.602	0.601	0.001
Agg. WTG 4	0.840	0.320	0.320	0.000	0.699	0.601	0.602	0.001

Table 4.13. *Simulation results for a bolted fault at the WTG 10 terminal (fault case 6), during normal operation (scenario 1) and contingency operation (scenario 2). All values are in p.u..*

	Scenario 1				Scenario 2			
Source	u	$i_{q,ref}$	$i_{q,sim}$	$i_{q,err}$	u	$i_{q,ref}$	$i_{q,sim}$	$i_{q,err}$
WTG 1	0.901	0.000	0.107	0.107	0.914	0.000	0.001	0.001
WTG 2	0.900	0.000	0.135	0.135	0.911	0.000	0.001	0.001
WTG 3	0.900	0.000	0.179	0.179	0.906	0.000	0.001	0.001
WTG 4	0.897	0.206	0.205	0.001	0.902	0.000	0.021	0.021
WTG 5	0.892	0.217	0.217	0.001	0.901	0.000	0.088	0.088
WTG 6	0.901	0.000	0.119	0.119	0.913	0.000	0.001	0.001
WTG 7	0.900	0.000	0.155	0.155	0.909	0.000	0.001	0.001
WTG 8	0.900	0.201	0.200	0.001	0.904	0.000	0.005	0.005
WTG 9	0.895	0.211	0.212	0.001	0.901	0.000	0.051	0.051
WTG 10	0.000	1.000	1.000	0.000	0.000	1.000	1.000	0.000
Agg. WTG 2	0.968	0.000	0.001	0.001	0.937	0.000	0.001	0.001
Agg. WTG 3	0.978	0.000	0.000	0.000	0.970	0.000	0.001	0.001
Agg. WTG 4	0.978	0.000	-0.001	0.001	0.970	0.000	0.001	0.001

Table 4.14. *Short-circuit calculation results for all short-circuited busbars and terminals (fault case 1-6), during normal operation (scenario 1).*

Fault location	I'_k [kA]	$I'_{k,\delta}$ [kA]	$i_{d.c.}$ [kA]	I_b [kA]	I_{th} [kA]	δ	t [s]
PCC	6.561	6.642	0.401	6.561	6.672	0.006	3
Onshore cable connection	4.982	5.169	1.383	4.982	5.143	0.019	2
Offshore platform 1	3.653	3.732	0.019	3.653	3.687	0.011	3
MV busbar 1	9.097	9.486	0.975	9.097	9.284	0.021	5
Array cable 1a terminal	7.995	8.294	0.150	7.995	8.094	0.019	13
WTG 10 terminal	48.321	50.065	2.107	48.321	49.060	0.018	142

Table 4.15. *Short-circuit calculation results for all short-circuited busbars and terminals (fault case 1-6), during normal operation (scenario 2).*

Fault location	I'_k [kA]	$I'_{k,\delta}$ [kA]	$i_{d.c.}$ [kA]	I_b [kA]	I_{th} [kA]	δ	t [s]
PCC	6.561	6.642	0.401	6.561	6.672	0.006	4
Onshore cable connection	4.982	5.169	1.383	4.982	5.143	0.019	2
Offshore platform 1	4.079	4.170	0.100	4.079	4.133	0.011	4
MV busbar 1	14.324	15.112	1.751	14.324	14.634	0.027	5
Array cable 1a terminal	12.465	12.795	0.114	12.465	12.597	0.013	16
WTG 10 terminal	49.308	49.772	2.095	49.308	50.057	0.005	36

4.3 Conclusions

From the obtained results in case study 1 and 2, it can be noted that the developed current source method provides results with reasonably low deviation from the expected value. A maximum deviation factor of 2.7 % was obtained in fault case 4, scenario 2. This is corresponding to a bolted fault applied at the MV busbar of the left branch in the system. One should keep in mind that there is always a level of interpretation involved when analyzing the simulation results, as well as understanding the arbitrary relative deviation measured by δ. As an example, consider the worst case performance of the method in fault case 4, scenario 2. Here, the bolted fault has separated the left branch of the OWPP from the right. The short-circuit current from the grid, as well as the aggregated WTGs of the right branch, are unaffected by the short-circuit current of the left branch. Because of this separation of the system, the results obtained for the right branch can be seen as locally converged, in the sense that a change of the short-circuit current in the left branch would have no effect on the right branch currents. The expected reactive short-circuit currents of the left branch WTGs are with most certainty 1.0 p.u., considering the extremely low terminal voltages. If the reactive short-circuit current in fact would converge to 1.0 p.u., the terminal voltage of the WTGs would increase. The change, however, would not alter the reference value, given the already extreme voltage sag. The expected reference value for a fully converged simulation could therefore be assumed to remain at 1.0 p.u.. Since this behavior generally only occurs for cases with extremely low terminal voltages, it therefore makes sense to refer to an expected reference value. This is, in other words, not a deterministic feature of the method, but rather based on the correlation between convergence issues and very low terminal voltages.

From the results in case study 1 and 2, one can also detect the effect of the smoothing function introduced by the current source method. Once again, the simulation results need to be interpreted by the user. The deviation caused by the smoothing function is measured using the deviation factor δ. Compared to the case mentioned in the above paragraph, it is much harder to make any claims about a true expected value for simulation results, such as the ones found in fault case 6, scenario 1. Consider the very narrow range of the reference curve for which these results are obtained. An incremental change in any of the sources could cause the reference value for any of the adjacent WTGs to change, to either side of the dead band. If the deviation factor for this case is compared to the worst case value obtained in fault case 4, scenario 2, it is lower. Since the deviation factor calculated in the worst case scenario is based on truly expected reference values, as explained above, it is of higher significance. This indicates that the estimated deviation occurring because of the smoothing function still is less, as compared with the worst case, even though it is not based on a true reference value. Overall, it can be concluded that the major source of error in the method is due to the saturation of the current sources, rather than the smoothing function.

The aggregated impedance model was shown to match the non-aggregated model with sufficient accuracy. One has to bear in mind that these results will depend on different fault scenarios, as the aggregated model is far from a perfect description of the system. Even though the aggregated model is effective for almost all relevant simulation cases, it can introduce high simulation errors because of the smoothing function used in the current source method. Once again, consider the results obtained for fault case 6, scenario 1. Here it was shown that even though a number of individual non-aggregated WTGs had large errors, the overall effect was relatively small. Instead, assume that the same terminal voltage was obtained when using an aggregated model, i.e. very close to 0.900 p.u.. The estimated error in the simulation results would then be higher, given that the aggregated WTG model contributes with a much higher short-circuit current, as compared to a handful of non-aggregated turbines. In the event of such a case, the simulation would have to be repeated with the aggregated model replaced by the non-aggregated. Since the non-aggregated turbines are separated by array cable impedances, the result would be closer to what is observed in fault case 6, scenario 1, thus mitigating the effect.

When comparing the results obtained in case study 1 and 2, it is clear that the overall system design will affect the simulation results. The choice of system impedances, as well as the strength of the external grid will have great impact on the level of short-circuit current and deviation factor δ.

Chapter 5

Final Remarks

In this chapter, a brief summary of the thesis is provided, as well as some general conclusions and recommendations. Lastly, possible future studies within the project are discussed.

5.1 Summary

In the process of designing offshore wind power plants, there are numerous studies that need to be performed. One of these studies are short-circuit studies. During a short-circuit, the system is subject to a sudden increase in current, due to a reduction of impedance. The short-circuit current will, depending on the duration of the fault, affect the system in different detrimental ways. Short-circuit studies are important since they are crucial for the dimensioning of transformers and breakers in the system. In order to be able to analyze numerous fault locations, and system configurations, so called static or steady-state short-circuit calculations are performed. These studies are approximate, as compared to more precise dynamic simulations. The benefit, however, is that they can be performed for a large number of test cases, with significantly less effort. There are a number of industry standards governing the calculation methods used for steady-state short-circuit studies.

Depending on the type of wind turbine generator utilized in the offshore wind power plant, the short-circuit contribution will be different. One type of such turbines are so called fully-rated converter wind turbine generators. These turbines are able to support the system during a fault through voltage regulation. By injecting a certain amount of reactive current, the turbines reduces the voltage sag during the fault, and thus, enables a faster recovery. When performing short-circuit studies, this behavior needs to be taken into account. One major issue, however, is that this behavior is not covered by the industry standards mentioned above.

In this master thesis project, a method used for steady-state short-circuit calculations in PowerFactory has been developed. The method aims to account for the

steady-state short-circuit behavior of fully-rated converter type wind turbine generators, complying with voltage control curves set by an arbitrary grid code. In order to do so, the current source model in PowerFactory has been utilized, and a special iterative algorithm implemented. To reduce simulation times, an aggregated wind turbine array model has been investigated and implemented. Two case studies were performed in order to evaluate and demonstrate the method. The first case study was a benchmark of the method, including a comparison with the current iteration method implemented in PowerFactory. The second case study illustrated a real-life short-circuit study of an offshore wind power plant. Overall, the obtained results showed a high level of accuracy, which was evaluated using a relative measurement of the deviation from the expected reference value. In general, it was concluded that the main source of error in simulation results were due to the inherit saturation of the current source, in addition to the smoothing function introduced by the method.

5.2 General Conclusions and Recommendations

In order for modern society to transition from conventional power sources, new and more sustainable technology need to be further developed. One example of such technology are wind power plants placed offshore. These power systems are under though constraints in terms of economical profitability and operations. If the grid code requirements of a TSO are to be met, while also providing profitable and safe system designs, the engineer needs to refine the calculation and simulation tools available. The method developed in this project is a small step towards more precise system designs.

The method developed for this project sufficiently handles simulation cases with a large group of FRC WTGs. In order to improve simulation times, multiple WTGs can be aggregated. Three types of errors have been identified in the method. The first one is the error introduced by the tolerance allowed in the iterative algorithm. Given the approximate nature of the steady-state calculations performed in this study, the deviations introduced by this tolerance are negligible. The second type of error is the deviation introduced by the smoothing function, used in the reference curve for the reactive current component. This effect can be mitigated by using non-aggregated WTG models. The third, and most severe type of error, is the deviation caused by the inherit saturation of the current source model in PowerFactory. For some types of short-circuit scenarios, the current sources will fail to obtain the target reactive current set by the reference value. This saturation normally occurs for cases when the terminal voltage of the WTG is very low. In order to evaluate the effect of these errors, the deviation factor δ was introduced. This factor measures the deviation from the expected WTG short-circuit currents relative to the short-circuit contribution of the external grid. From simulations, it was found that the worst case value of δ was 2.7 % for a system resembling a realistic OWPP.

It is recommended that the user of the current source method is familiarized with the implications of δ, while also understanding the error sources found within the method. The conservative estimate of the short-circuit current $I'_{k,\delta}$, is provided to increase the conservativeness of the short-circuit analysis. This estimate is scaled based on the relative error of the short-circuit currents produced by the WTGs. With this in mind, it is worth pointing out that the estimate is based on the worst case scenario, where a portion of the WTGs short-circuit contribution is completely canceling out a part of the grid current. For the case mentioned in the paragraph above, this corresponds to an increase of 5.4 % in the total short-circuit. Consider the opposite case, where the same portion of the WTG short-circuit contribution is superposed to the grid current. Analogous, the simulated total short-circuit current I'_k would thus be 5.4 % higher than the "true" value. In other words, there is an error tolerance of $2 \times 5.2 = 10.8$ % for this specific case. In general, this corresponds to $4 \times \delta$. I.e. when using the conservative estimate $I'_{k,\delta}$, the user needs to be aware of the risk of obtaining a total short-circuit current which is $4 \times \delta$ too high. Naturally, this statement will only be valid under the assumption that all other values within the simulation are correctly obtained.

5.3 Future Studies

In order to further develop the current source method, a number of improvements are suggested.

The most crucial improvement to the proposed method, is to develop a more refined short-circuit model of the grid. Consider the fact that the grid still contributes with a major portion of the short-circuit current. If this model is inaccurate, or somehow erroneous, its impact on the total short-circuit current will be much higher than the estimated contribution of the wind turbine generators. Since the short-circuit behavior of the WTGs is very much depending on the short-circuit current of the grid, this would also imply that the FRC WTG short-circuit contribution is faulty as well.

Naturally, the algorithm could be further tweaked, to improve simulation times and avoid cases when the nudge factor k_n needs to be utilized. To enhance the method, and make it better suited for future short-circuit studies, the algorithm used for the reference voltage control curve could be further adjusted, to account for a greater selection of arbitrary shapes, such as multiple slopes and break points.

Furthermore, more effort could be spent dealing with the other relevant current components briefly discussed in this thesis. One key component omitted from this study is the peak current. There are two suggested ways to proceed. The first one is to find a general formula through which the peak current can be post-calculated, much like what is done in the IEC 60909 standard. This formula would have to be

fitted to results obtained through dynamic simulations. The second suggestion is to include other PowerFactory components, such as a voltage source or a synchronous generator, which possibly could capture the expected peak current behavior of a given FRC WTG model. This would require further expansion of the iterative method, to incorporate additional PowerFactory models.

A greater number of steady-state short-circuit case studies could be performed in order to validate the method, and its relative sensitivity to changes in the system impedances and external grid model. Since there was no real-life data available for the external grid model in the second case study, more extensive research could be performed, to further validate the effectiveness of the current source method. Given the limited size of the second case study, a much larger OWPP could also be analyzed in order to validate the method.

In order to truly validate the method, however, numerous dynamic simulations should be performed. These results should be compared with results obtained when using the steady-state calculation method found in this project. The dynamic results could also help to validate other short-circuit current components, such as the decaying DC component, which for this study has been assumed to be zero. Also, the dynamic simulations could help to establish the peak current behavior of the FRC WTG, as mentioned above.

Acronyms

AC	Alternating Current.
DC	Direct Current.
DFAG	Doubly-fed Asynchronous Generator.
DFIG	Doubly-fed Induction Generator.
DIgSILENT	Digital SimuLator for Electrical NeTwork.
DVS	Dynamic Voltage Support.
FRC	Fully-Rated Converter.
FRC WTG	Fully-Rated Converter Wind Turbine Generator.
HVAC	High Voltage Alternating Current.
HVDC	High Voltage Direct Current.
IEC	International Electrotechnical Commission.
LVRT	Low-Voltage-Ride-Through.
OLTC	On-Load Tap Changer.
OWC	Offshore Wind Connections, part of the Power System Division at ABB.
OWPP	Offshore Wind Power Plant.
p.u.	Per Unit.
PCC	Point of Common Connection.
PMSG	Permanent Magnet Synchronous Generator.
RMS	Root Mean Square.

SCIG Squirrel Cage Induction Generator.
SCR Short-Circuit Ratio.
SMIB Single-Machine Infinite Bus.

TSO Transmission System Operator.

VDE Verband der Elektrotechnik Elektronik Informationstechnik e.V..

WRIG Wound-rotor Induction Generator.
WTG Wind Turbine Generator.

List of Symbols

i_{cap}	Type of output current of the PowerFactory current source model (capacative or inductive).
i_{setp}	Current set point of the PowerFactory current source model [p.u.].
k	Alteration coefficient used in iterative algorithm.
ϕ	Power angle.
$\cos\phi$	Power factor.
$\boldsymbol{I_b}$	Symmetrical breaking current.
$\boldsymbol{i_{d.c.}}$	Decaying DC component.
I_n	Nominal WTG current.
$\boldsymbol{i_p}$	Peak current.
$\boldsymbol{I''_k}$	Initial or subtransient symmetrical short-circuit current.
$\boldsymbol{I'_k}$	Transient symmetrical short-circuit current.
$\boldsymbol{I_k}$	Steady-state short-circuit current.
$I'_{k,\delta}$	Conservative estimate of the resulting short-circuit current.
$\boldsymbol{I_{th}}$	Thermal equivalent current.
I_{eq}	Equivalent WTG array current.
Z_{eq}	Equivalent WTG array impedance.
f_c	Equivalent frequency used for calculation of the equivalent impedance $\boldsymbol{Z_c}$.
$\boldsymbol{Z_c}$	Equivalent impedance used for calculation of the short-circuit peak current.
$\boldsymbol{Z_f}$	Fault impedance.

κ	Factor used for calculation of short-circuit peak current.
$\boldsymbol{Z_Q}$	Short-circuit impedance of a network feeder.
$I''_{k,Q}$	Rated subtransient short-circuit current of a network feeder.
$U_{n,Q}$	Nominal voltage at the connection of a network feeder.
U_n	Nominal voltage.
k_n	Nudge factor used in the iterative algorithm of the current source method.
δ	Deviation factor.
Δu	WTG terminal voltage drop [p.u.].
i_d	Active current [p.u.].
$i_{d,ref}$	Active reference current [p.u.].
i_{max}	Maximum reference current [p.u.].
i_q	Reactive current [p.u.].
$i_{d,max}$	Maximum active reference current [p.u.].
$i_{q,max}$	Maximum reactive reference current [p.u.].
$i_{q,min}$	Minimum reactive reference current [p.u.].
$i_{q,ref}$	Reactive reference current [p.u.].
K	Slope of voltage control reference curve.
n	Polynomial degree of smoothing function.
u_{DB}	Dead band voltage [p.u.].
ξ	Error factor used for calculating δ.
$\boldsymbol{Z_k}$	Equivalent short-circuit impedance of a network.
S''_k	Subtransient short-circuit power level.
u_{Rr}	Rated resistive component of the short-circuit voltage in per cent.
u_{kr}	Short-circuit voltage at rated current in per cent.
Z_T	Short-circuit impedance of a transformer.
K_T	Transformer correction factor.
$S_{n,T}$	Transformer power rating.
$U_{n,T}$	Transformer voltage rating referred to either the high or low voltage side.

x_T	Relative reactance of transformer in p.u..
c_{max}	Voltage factor used for calculation of maximum short-circuit current.

Bibliography

[1] European Commission, "The eu climate and energy package." http://ec.europa.eu/clima/policies/package/.

[2] D. Gross and F. Roth, *The Europe 2020 Strategy*. Centre for European Policy Studies (CEPS), 2012.

[3] K. Bruninx, D. Madzharov, E. Delarue, and W. D'haeseleer, "Impact of the german nuclear phase-out on europe's electricity generation," in *European Energy Market (EEM), 2012 9th International Conference on the*, pp. 1–10, 2012.

[4] International Energy Agency and Organisation for Economic Co-operation and Development, "Chapter 7: Renewable energy outlook," in *World Energy Outlook 2012*, WORLD ENERGY OUTLOOK, Organization for Economic Cooperation & Development, 2012.

[5] L. Wang, J. Wei, X. Wang, and X. Zhang, "The development and prospect of offshore wind power technology in the world," in *World Non-Grid-Connected Wind Power and Energy Conference, 2009. WNWEC 2009*, pp. 1–4, 2009.

[6] C. Bak, "Power system technical performance issues related to the application of long hvac cables," *Electra*, vol. 270, 2013.

[7] H. Polinder, J. Ferreira, B. Jensen, A. Abrahamsen, K. Atallah, and R. McMahon, "Trends in wind turbine generator systems," *Emerging and Selected Topics in Power Electronics, IEEE Journal of*, vol. 1, no. 3, pp. 174–185, 2013.

[8] G. Ramtharan, A. Arulampalam, J. Ekanayake, F. Hughes, and N. Jenkins, "Fault ride through of fully rated converter wind turbines with ac and dc transmission," *Renewable Power Generation, IET*, vol. 3, no. 4, pp. 426–438, 2009.

[9] H. Mokui, M. Mohseni, and M. A. S. Masoum, "Investigating the transient responses of fully rated converter-based wind turbines," in *Universities Power Engineering Conference (AUPEC), 2011 21st Australasian*, pp. 1–7, 2011.

[10] International Electrotechnical Commission, *IEC 60909-0: Short-circuit currents in three-phase a.c. systems - Part 0: Calculations of currents*, 2001. IEC 60909-0:2001(E).

[11] "Chapter 22: Short-circuit analysis," in *DIgSILENT PowerFactory v. 15 - User Manual (Online Edition)*, pp. 429–462, DIgSILENT GmbH, February, 2013.

[12] B. Tounsi, A. Henry, and L. Vanfretti, "Modelling and dynamic analysis of offshore wind farms according to the french tso grid code," in *IECON 2012 - 38th Annual Conference on IEEE Industrial Electronics Society*, pp. 1374–1380, 2012.

[13] A. Ellis, R. Nelson, E. Von Engeln, R. Walling, J. MacDowell, L. Casey, E. Seymour, W. Peter, C. Barker, B. Kirby, and J. R. Williams, "Reactive power performance requirements for wind and solar plants," in *Power and Energy Society General Meeting, 2012 IEEE*, pp. 1–8, 2012.

[14] S. Chondrogiannis, M. Barnes, M. Aten, and P. Cartwright, "Modelling and gb grid code compliance studies of offshore wind farms with doubly-fed induction generators," in *Power Electronics, Machines and Drives, 2006. The 3rd IET International Conference on*, pp. 22–26, 2006.

[15] M. Tsili and S. Papathanassiou, "A review of grid code technical requirements for wind farms," *Renewable Power Generation, IET*, vol. 3, no. 3, pp. 308–332, 2009.

[16] H. Guo, K. Rudion, and Z. Styczynski, "Integration of large offshore wind farms into the power system," in *Science and Technology, 2011 EPU-CRIS International Conference on*, pp. 1–6, 2011.

[17] M. Mohseni and S. Islam, "International regulations on the transient response of large wind power plants," in *IECON 2011 - 37th Annual Conference on IEEE Industrial Electronics Society*, pp. 3164–3169, 2011.

[18] E. Muljadi, N. Samaan, V. Gevorgian, J. Li, and S. Pasupulati, "Short circuit current contribution for different wind turbine generator types," in *Power and Energy Society General Meeting, 2010 IEEE*, pp. 1–8, 2010.

[19] Y. Wang, J. Li, S. Hu, and H. Xu, "Analysis on dfig wind power system low-voltage ridethrough," in *Artificial Intelligence, 2009. JCAI '09. International Joint Conference on*, pp. 676–679, 2009.

[20] R. J. Nelson and H. Ma, "Short-circuit contributions of full-converter wind turbines," in *Power and Energy Society General Meeting, 2011 IEEE*, pp. 1–4, 2011.

[21] M. Valentini, "Fault current contribution from vsc-based wind turbines to the grid," Master's thesis, Aalborg University, 2008.

[22] S. Chen, T. Lund, M. Zamastil, V. Akhmatov, H. Abildgaard, and B. Gellert, "Short-circuit calculations considering converter-controlled generation components," in *Energytech, 2012 IEEE*, pp. 1–6, 2012.

[23] Energinet.dk, *Technical regulation 3.2.5 for wind power plants with a power output greater than 11 kW*, September 2010. 55986/10,.

[24] DIgSILENT GmbH, *DIgSILENT Technical Documentation: What's New in PowerFactory Version 14.1*, August 2011.

[25] M. Pöller, "Modelling of wind generation for fault level studies," in *1st Wind Integration Symposium*, DIgSILENT GmbH, Frankfurt 2011.

[26] E. Muljadi, S. Pasupulati, A. Ellis, and D. Kosterov, "Method of equivalencing for a large wind power plant with multiple turbine representation," in *Power and Energy Society General Meeting - Conversion and Delivery of Electrical Energy in the 21st Century, 2008 IEEE*, pp. 1–9, 2008.

[27] H. Li and Z. Chen, "Overview of different wind generator systems and their comparisons," *Renewable Power Generation, IET*, vol. 2, no. 2, pp. 123–138, 2008.

[28] H. Polinder, "Overview of and trends in wind turbine generator systems," in *Power and Energy Society General Meeting, 2011 IEEE*, pp. 1–8, 2011.

[29] F. Blaabjerg and K. Ma, "Future on power electronics for wind turbine systems," *Emerging and Selected Topics in Power Electronics, IEEE Journal of*, vol. 1, no. 3, pp. 139–152, 2013.

[30] F. Blaabjerg, Z. Chen, and S. Kjaer, "Power electronics as efficient interface in dispersed power generation systems," *Power Electronics, IEEE Transactions on*, vol. 19, no. 5, pp. 1184–1194, 2004.

[31] Z. Chen and E. Spooner, "Voltage source inverters for high-power, variable-voltage dc power sources," *Generation, Transmission and Distribution, IEE Proceedings-*, vol. 148, no. 5, pp. 439–447, 2001.

[32] I. Lar, M. Radulescu, E. Ritchie, and A. A. Pop, "Current control methods for grid-side three-phase pwm voltage-source inverter in distributed generation systems," in *Optimization of Electrical and Electronic Equipment (OPTIM), 2012 13th International Conference on*, pp. 859–867, 2012.

[33] D. Lijie, L. Yang, and M. Yiqun, "Comparison of high capacity svc and statcom in real power grid," in *Intelligent Computation Technology and Automation (ICICTA), 2010 International Conference on*, vol. 1, pp. 993–997, 2010.

[34] S.-F. Chou, C.-T. Lee, P.-T. Cheng, and F. Blaabjerg, "A reactive current injection technique for renewable energy converters in low voltage ride-through operations," in *Power and Energy Society General Meeting, 2011 IEEE*, pp. 1–7, 2011.

[35] E.ON Netz GmbH, *Grid Code for high and extra high voltage*, 1st ed., 2006.

[36] L. Wang, C.-J. Yeh, M.-H. Hsieh, C.-T. Wu, and C.-L. Lu, "Analysis of voltage variations and short-circuit ratios of a large-scale offshore wind farm connected to a practical power system," in *Power and Energy Society General Meeting (PES), 2013 IEEE*, pp. 1–5, 2013.

[37] J. Feltes and B. S. Fernandes, "Wind turbine generator dynamic performance with weak transmission grids," in *Power and Energy Society General Meeting, 2012 IEEE*, pp. 1–7, 2012.

[38] J. O. Tande, G. D. Marzio, and K. Uhlen, "System requirements for wind power plants," tech. rep., SINTEF Energy Research, november 2007.

[39] F. Iov, A. D. Hansen, P. Sørensen, and N. A. Cutululis, "Mapping of grid faults and grid codes," Tech. Rep. Risø-R-1617(EN), RisøNational Laboratory - Technical University of Denmark, July 2007. ISSN 0106-2840, ISBN 978-87-550-3622-2.